Engineering Fracture Mechanics 78 (2011) 27–46

Contents lists available at ScienceDirect

Engineering Fracture Mechanics

journal homepage: www.elsevier.com/locate/engfracmech

Stochastic multiscale fracture analysis of three-dimensional functionally graded composites

Sharif Rahman [a,*], Arindam Chakraborty [b]

[a] Department of Mechanical and Industrial Engineering, The University of Iowa, Iowa City, IA 52242, USA
[b] Structural Integrity Associates, Inc., 5215 Hellyer Avenue, Suite 210, San Jose, CA 95138, USA

ARTICLE INFO

Article history:
Received 9 October 2009
Received in revised form 2 September 2010
Accepted 13 September 2010
Available online 19 September 2010

Keywords:
Probabilistic fracture mechanics
Polynomial dimensional decomposition
Random microstructure
Reliability

ABSTRACT

A new moment-modified polynomial dimensional decomposition (PDD) method is presented for stochastic multiscale fracture analysis of three-dimensional, particle-matrix, functionally graded materials (FGMs) subject to arbitrary boundary conditions. The method involves Fourier-polynomial expansions of component functions by orthonormal polynomial bases, an additive control variate in conjunction with Monte Carlo simulation for calculating the expansion coefficients, and a moment-modified random output to account for the effects of particle locations and geometry. A numerical verification conducted on a two-dimensional FGM reveals that the new method, notably the univariate PDD method, produces the same crude Monte Carlo results with a five-fold reduction in the computational effort. The numerical results from a three-dimensional, edge-cracked, FGM specimen under a mixed-mode deformation demonstrate that the statistical moments or probability distributions of crack-driving forces and the conditional probability of fracture initiation can be efficiently generated by the univariate PDD method. There exist significant variations in the probabilistic characteristics of the stress-intensity factors and fracture-initiation probability along the crack front. Furthermore, the results are insensitive to the subdomain size from concurrent multiscale analysis, which, if selected judiciously, leads to computationally efficient estimates of the probabilistic solutions.

1. Introduction

In functionally graded materials (FGMs), the introduction of gradual changes in material compositions and microstructures at the macroscale removes large-scale, interface-induced stress singularities that can otherwise lead to delamination failure [1]. However, due to formation of cracks during processing or service life, fracture remains an important failure mechanism. There are two major challenges in conducting fracture analyses of FGMs. First, an FGM is a multiphase, heterogeneous material with multiscale features, which, depending on the crack-tip location and microstructure, can have markedly different crack-driving forces. Second, the microstructure of an FGM is inherently stochastic, which can be modeled as a random field, describing random distributions of sizes, shapes, and orientations of constituent phases. Therefore, stochastic multiscale models are ultimately necessary to provide a realistic computational framework for determining mechanical performance of a crack, real or postulated, in an FGM.

Past computational works on FGM fracture are primarily driven by deterministic macroscopic models and entail mostly two-dimensional [2–4] and a few three-dimensional [5–7] media for calculating the stress-intensity factors (SIFs) from

* Corresponding author. Tel.: +1 319 335 5679.
E-mail address: rahman@engineering.uiowa.edu (S. Rahman).

0013-7944/$ - see front matter © 2010 Elsevier Ltd. All rights reserved.
doi:10.1016/j.engfracmech.2010.09.006

spatially varying elastic properties. In contrast, models of random microstructure or multiscale fracture analysis are few and far between [8,9], and they mostly delve into two-dimensional FGMs. For instance, the authors recently developed a concurrent multiscale model, which includes a stochastic description of a two-dimensional FGM microstructure and constituent material properties, a two-scale algorithm including microscale and macroscale analyses for determining crack-driving forces, and crude Monte Carlo simulation for fracture reliability analysis [9]. Numerical results indicate that the concurrent multiscale model is sufficiently accurate, gives fracture probability solutions very close to those generated from the microscale (reference) model, and can reduce the computational effort of the latter model by a factor of more than two. However, the stochastic analysis in both multiscale and microscale models was conducted using crude Monte Carlo simulation, requiring tens of thousands of deterministic finite-element analyses (FEA) to estimate tail probabilities. In other words, the increased computational speed gained by the multiscale model is due to more efficient FEA in each deterministic sample, not stochastic analysis. Therefore, further research exploiting alternative stochastic methods – the principal objective of this work – should pave the way for probabilistic fracture analysis in a computationally efficient way. Developing such alternative methods becomes indispensable when analyzing cracks in three-dimensional FGMs, as crude Monte Carlo simulation is no longer a viable option due to increased computational demand from three-dimensional FEA.

This paper presents a new moment-modified polynomial dimensional decomposition (PDD) method for stochastic multiscale fracture analysis of three-dimensional, particle-matrix FGMs subject to arbitrary boundary conditions. The method is based on (1) Fourier-polynomial expansions of component functions by orthonormal polynomial bases, (2) an additive control variate in conjunction with Monte Carlo simulation for efficient calculation of the expansion coefficients, and (3) a moment-modified random output to account for the effects of particle locations and geometry. Section 2 describes a generic, stochastic FGM fracture problem, defines random input parameters, and discusses crack-driving forces. Section 3 presents a concurrent multiscale model for fracture analysis. Section 4 explores PDD, presents an efficient method for calculating the expansion coefficients, including a moment-modified random output, and discusses computational effort. The section also includes numerical results from a two-dimensional FGM analysis, essentially verifying the PDD method. Section 5 illustrates the capability of the proposed method by solving a three-dimensional FGM fracture problem, leading to the statistical moments and probability densities of crack-driving forces and the conditional probability of fracture initiation. Finally, the conclusions are drawn in Section 6.

2. Stochastic fracture problem

Consider a two-phase, functionally graded, heterogeneous solid with a planar crack, domain $\mathscr{D} \subset \mathbb{R}^3$, and a schematic illustration of its microstructure, as shown in Fig. 1a. [1]The microstructure includes two distinct material phases, phase p (green or dark) and phase m (white or light), denoting particle and matrix constituents with subdomains $\mathscr{D}_p \subset \mathscr{D}$ and $\mathscr{D}_m \subset \mathscr{D}$, respectively, where $\mathscr{D}_p \cup \mathscr{D}_m = \mathscr{D}$ and $\mathscr{D}_p \cap \mathscr{D}_m = \emptyset$. Both constituents represent isotropic and linear-elastic materials, and the elasticity tensors of the particle and matrix, denoted by $\boldsymbol{C}^{(p)}$ and $\boldsymbol{C}^{(m)}$, respectively, are

$$\boldsymbol{C}^{(i)} := \frac{\nu_i E_i}{(1+\nu_i)(1-2\nu_i)}\mathbf{1}\otimes\mathbf{1} + \frac{E_i}{(1+\nu_i)}\boldsymbol{I}; \quad i = p, m, \tag{1}$$

where the symbol $\otimes$ denotes the tensor product; E_i and ν_i are the elastic modulus and Poisson's ratio, respectively, of phase i; and $\mathbf{1}$ and $\boldsymbol{I}$ are second- and fourth-rank identity tensors, respectively. The superscripts or subscripts $i = p$ and $i = m$ refer to particle and matrix, respectively. At a spatial point $\boldsymbol{x} \in \mathscr{D}$ in the macroscopic length scale, let $\phi_p(\boldsymbol{x})$and $\phi_m(\boldsymbol{x})$ denote the volume fractions of the particle and matrix, respectively. Each volume fraction is bounded between 0 and 1 and satisfies the constraint $\phi_p(\boldsymbol{x}) + \phi_m(\boldsymbol{x}) = 1$. The crack faces are traction-free, and there is perfect bonding between the matrix and particles. In addition, no porosities are included in the matrix or particle phases.

For a quasi-static, elastic problem with small displacements and strains, the variational or weak form of the equilibrium equation and boundary conditions is

$$\int_{\mathscr{D}} (\boldsymbol{C}(\boldsymbol{x}) : \boldsymbol{\epsilon}) : \delta\boldsymbol{\epsilon}\, d\mathscr{D} - \int_{\mathscr{D}} \boldsymbol{b}\cdot\delta\boldsymbol{u}\, d\mathscr{D} - \int_{\Gamma_t} \bar{\boldsymbol{t}}\cdot\delta\boldsymbol{u}\, d\Gamma - \sum_{\boldsymbol{x}_K\in\Gamma_u} \boldsymbol{f}(\boldsymbol{x}_K)\cdot\delta\boldsymbol{u}(\boldsymbol{x}_K) - \sum_{\boldsymbol{x}_K\in\Gamma_u} \delta\boldsymbol{f}(\boldsymbol{x}_K)\cdot[\boldsymbol{u}(\boldsymbol{x}_K) - \bar{\boldsymbol{u}}(\boldsymbol{x}_K)] = 0, \tag{2}$$

where $\boldsymbol{u} : \mathscr{D} \to \mathbb{R}^3$ is the displacement vector; $\boldsymbol{C}(\boldsymbol{x})$ and $\boldsymbol{\epsilon} := (1/2)(\nabla + \nabla^T)\boldsymbol{u}$ denote the spatially variant elasticity tensor and strain tensor, respectively; Γ_t and Γ_u are two disjoint portions of the boundary Γ, where the traction vector $\bar{\boldsymbol{t}}$ and displacement $\bar{\boldsymbol{u}}$ are prescribed, respectively; $\boldsymbol{f}^T(\boldsymbol{x}_K)$ is the vector of reaction forces at a constrained node K on Γ_u; $\nabla^T := \{\partial/\partial x_1, \partial/\partial x_2, \partial/\partial x_3\}$ is the vector of gradient operators; and symbols ".", ":", and δ denote dot product, tensor contraction, and variation operator, respectively. The discretization of the weak form, Eq. (2), depends on how the elasticity tensor $\boldsymbol{C}(\boldsymbol{x})$ is defined, *i.e.*, how the elastic properties of constituent material phases and their gradation characteristics are described. Nonetheless, a numerical method, *e.g.*, the finite-element method, is generally required to solve the discretized weak form, providing various response fields of interest.

[1] For interpretation of color in Figs. 1 and 3–10, the reader is referred to the web version of this article.

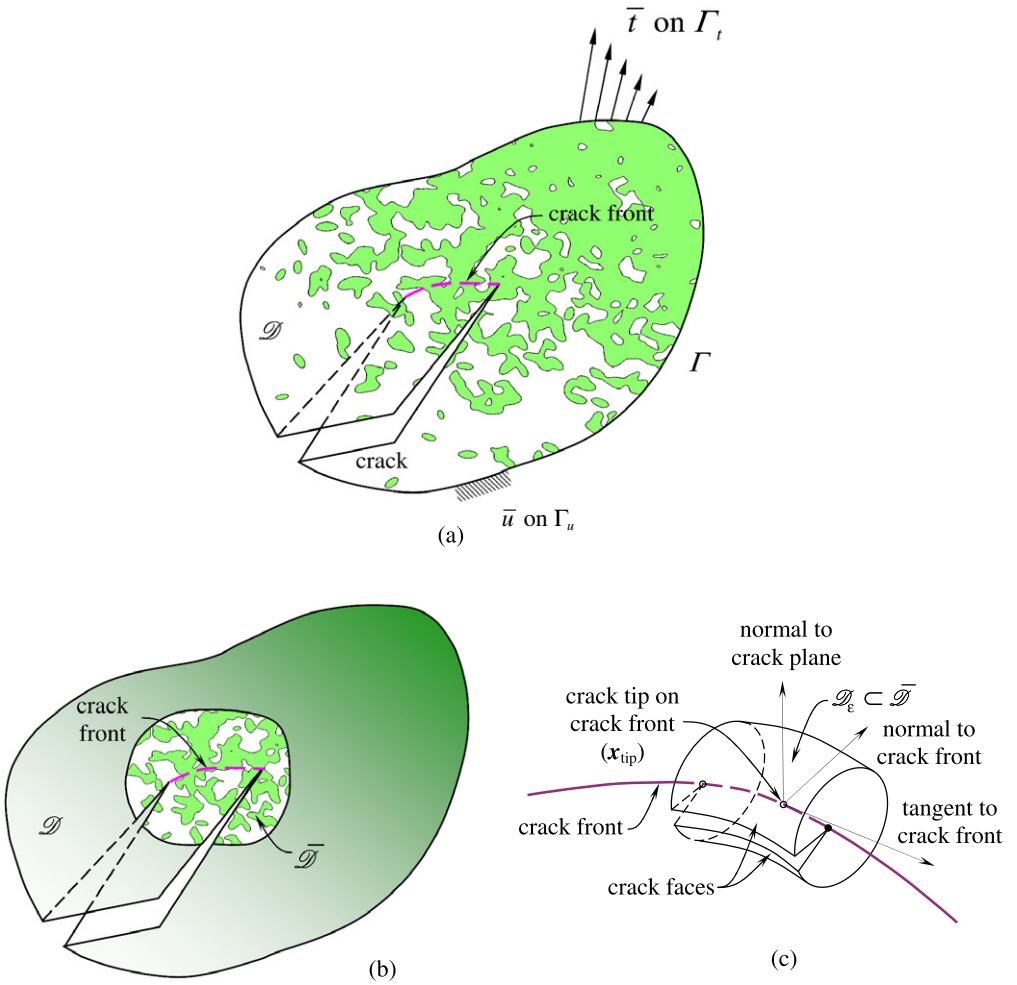

Fig. 1. Schematics of a two-phase, three-dimensional FGM fracture problem: (a) a planar crack subject to arbitrary boundary conditions; (b) a concurrent multiscale model; and (c) a small, bounded subdomain of a crack tip. Note: $\mathscr{D}$ = domain of the entire solid, $\bar{\mathscr{D}}$ = subdomain with explicit microstructure, $\mathscr{D}_\epsilon$ = small subdomain surrounding a crack tip on the crack front.

2.1. Random input

Uncertainties in input to FGM fracture analysis leading to statistical characteristics of SIFs come from a variety of sources. Two important sources considered in this work are: (1) random microstructure, including uncertainties in the volume fraction, number, and locations of particles and (2) random elastic material properties of constituents. They are briefly described as follows.

2.1.1. Random microstructure

2.1.1.1. Particle volume fraction. The particle volume fraction $\phi_p(\boldsymbol{x})$ can be modeled as an inhomogeneous (non-stationary), non-Gaussian, random field, which has mean $\mu_p(\boldsymbol{x})$ and standard deviation $\sigma_p(\boldsymbol{x})$ [10]. The standardized particle volume fraction

$$\tilde{\phi}_p(\boldsymbol{x}) := \frac{\phi_p(\boldsymbol{x}) - \mu_p(\boldsymbol{x})}{\sigma_p(\boldsymbol{x})}, \tag{3}$$

which has zero mean and unit variance, is at least a weakly homogeneous (stationary) random field with prescribed covariance function $\Gamma_{\tilde{\phi}_p}(\boldsymbol{s}) := \mathbb{E}\left[\tilde{\phi}_p(\boldsymbol{x})\tilde{\phi}_p(\boldsymbol{x}+\boldsymbol{s})\right]$, where $\mathbb{E}$ is the expectation operator, and with marginal cumulative distribution function $F_p(\tilde{\phi}_p)$ such that $0 \leqslant \phi_p(\boldsymbol{x}) \leqslant 1$ with probability one. If the covariance function $\Gamma_{\tilde{\phi}_p}(\boldsymbol{s})$ is appropriately bounded, the standardized phase volume fraction can be viewed as a translation random field $\tilde{\phi}_p(\boldsymbol{x}) = G_p[\alpha_p(\boldsymbol{x})] := F_p^{-1}[\Phi(\alpha_p(\boldsymbol{x}))]$, where G_p is a mapping of the Gaussian field on a non-Gaussian field, $\alpha_p(\boldsymbol{x})$ is the Gaussian image field, and $\Phi(\cdot)$ is the distribution function of a standard Gaussian random variable. Subsequently, the Karhunen–Loéve approximation of the image field leads to [10]

$$\tilde{\phi}_p(\boldsymbol{x}) \cong G_p\left[\sum_{k=1}^{M} Z_{p,k}\sqrt{\lambda_{p,k}}\Psi_{p,k}(\boldsymbol{x})\right], \tag{4}$$

where $\lambda_{p,k}$ and $\Psi_{p,k}(\boldsymbol{x})$ denote the k^{th} eigenvalue and the k^{th} eigenfunction, respectively, of the covariance function of $\alpha_p(\boldsymbol{x})$, and $Z_{p,k}$ is an independent copy of a standard Gaussian random variable. According to Eq. (4), the Karhunen–Loéve approximation yields a parametric representation of the standardized phase volume fraction $\check{\phi}_p(\boldsymbol{x})$ and, hence, of $\phi_p(\boldsymbol{x})$ with M Gaussian variables. The random field description of $\phi_p(\boldsymbol{x})$ allows the particle volume fraction to have random fluctuations at a point $\boldsymbol{x}$ in the macroscopic length scale.

2.1.1.2. Particle number and locations. The random microstructure entailing particle locations can be described using the well-known Poisson random field. However, since the FGM microstructure varies spatially, the Poisson field must be inhomogeneous. Consider an inhomogeneous Poisson field $\mathcal{N}(\mathscr{D}')$ with an intensity measure $\mu_{\mathscr{D}'} := \int_{\mathscr{D}'} \lambda(\boldsymbol{x})\, d\boldsymbol{x}$, where $\boldsymbol{x} \in \mathscr{D}' \subset \mathbb{R}^3$ is a spatial coordinate, $\lambda(\boldsymbol{x}) \geqslant 0$ is a spatially variant intensity function, and $\mathscr{D}' \in \mathbb{R}^3$ is a bounded subset of $\mathbb{R}^3$ such that points of $\mathcal{N}$ falling in $\mathbb{R}^3 \setminus \mathscr{D}'$ do not contribute to particles in $\mathscr{D}$. The Poisson point field has the following properties: (1) the number $\mathcal{N}(\mathscr{D}')$ of points in a bounded subset $\mathscr{D}'$ has a Poisson distribution with intensity measure $\mu_{\mathscr{D}'}$; and (2) random variables $\mathcal{N}(\mathscr{D}'_1), \ldots, \mathcal{N}(\mathscr{D}'_K)$ for any integer $K \geqslant 2$ and disjoint sets $\mathscr{D}'_1, \ldots, \mathscr{D}'_K$ are statistically independent. The Poisson field $\mathcal{N}(\mathscr{D}')$ gives the number of points in $\mathscr{D}'$ and is characterized by the probability,

$$P[\mathcal{N}(\mathscr{D}') = n] = \frac{\left(\int_{\mathscr{D}'} \lambda(\boldsymbol{x})\, d\boldsymbol{x}\right)^n}{n!} \exp\left(-\int_{\mathscr{D}'} \lambda(\boldsymbol{x})\, d\boldsymbol{x}\right); \quad n = 0, 1, 2, \ldots, \tag{5}$$

that n Poisson points exist in $\mathscr{D}'$. An FGM with fully penetrable spherical particles that have the same deterministic size, as assumed in this work, and a deterministic particle volume fraction $\varphi_p(\boldsymbol{x})$ has the intensity function [11]

$$\lambda(\boldsymbol{x}) \cong \frac{1}{V_p} \ln\left[\frac{1}{1 - \varphi_p(\boldsymbol{x})}\right]; \ \boldsymbol{x} \in \mathscr{D}', \tag{6}$$

where V_p is the common volume of the particles. When $\phi_p(\boldsymbol{x})$ is a random field, as treated in this work, $\varphi_p(\boldsymbol{x})$ can be viewed as a sample function of $\phi_p(\boldsymbol{x})$. For more complex microstructures comprising random particle geometry, no such closed-form relationships exist, but they can be formulated algorithmically [12].

2.1.1.3. Mosaic random field. A random point field, known as the mosaic random field [13] and employing an inhomogeneous Poisson field, can be used to model particle-matrix FGMs. Once the intensity function has been determined, samples of synthetic microstructures of two-phase FGMs are generated from the mosaic random field based on the following algorithm:

- Step 1: Define bounded subsets $\mathscr{D}$ and $\mathscr{D}'$ of $\mathbb{R}^3$. The bounded subset $\mathscr{D}'$ must be such that points of $\mathcal{N}$ falling in $\mathbb{R}^3 \setminus \mathscr{D}'$ do not contribute to particles in $\mathscr{D}$.
- Step 2: Generate a sample $\varphi_p(\boldsymbol{x})$ of the random particle volume fraction $\phi_p(\boldsymbol{x})$ using Eqs. (3) and (4). Calculate the corresponding sample $\lambda(\boldsymbol{x})$ of the random intensity function from Eq. (6).
- Step 3: Generate a sample k^* of the homogeneous Poisson random variable $N^*(\mathscr{D}')$, which has a constant intensity $\lambda^* = \max_{\boldsymbol{x} \in \mathbb{R}^3} \lambda(\boldsymbol{x})$, where $\lambda(\boldsymbol{x})$ is a bounded intensity function in $\mathscr{D}'$.
- Step 4: Generate k^* independent samples of uniformly distributed points $(u_{i,1}, u_{i,2}, u_{i,3})$ in $\mathscr{D}'$. Denote these points by $\boldsymbol{x}_i$, $i = 1, \ldots, k^*$.
- Step 5: Perform thinning of the point set obtained in Step 4. In so doing, each point $\boldsymbol{x}_i$, independently of the other, is kept with probability $\lambda(\boldsymbol{x}_i)/\lambda^*$, which is equivalent to discarding the point with probability $1 - \lambda(\boldsymbol{x}_i)/\lambda^*$. The resulting point pattern with the size $k \leqslant k^*$ follows the inhomogeneous Poisson field $\mathcal{N}(\mathscr{D}')$ with the intensity function $\lambda(\boldsymbol{x})$. Let these points be denoted by $\boldsymbol{\Gamma}_i$, $i = 1, \ldots, k$.
- Step 6: Place particles with their centroids coincident with the points $\boldsymbol{\Gamma}_i$, $i = 1, \ldots, k$. The resultant subsets $\mathscr{D}_p$ and $\mathscr{D}_m$ of the particle and matrix regions, respectively, of $\mathscr{D}$ produce a sample of a two-phase, statistically inhomogeneous microstructure.

Independent samples of an FGM random microstructure are delivered by repeated application of the above algorithm.

2.1.2. Random constituent material properties

In addition to a spatially variant random volume fraction of particles leading to a random microstructure, the constituent properties of material phases can also be stochastic. Let E_p and ν_p denote the elastic modulus and Poisson's ratio, respectively, of the particle, and E_m and ν_m denote the elastic modulus and Poisson's ratio, respectively, of the matrix. Therefore, the random vector $\{E_p, E_m, \nu_p, \nu_m\}^T \in \mathbb{R}^4$ describes the stochastic elastic properties of both constituents. Unlike volume fractions, however, the constituent properties are spatially invariant in the macroscopic length scale.

In summary, the input uncertainties include: (1) M random variables $Z_{p,1}, \ldots, Z_{p,M}$ due to the discretization of the random field $\phi_p(\boldsymbol{x})$; (2) a Poisson random variable $\mathcal{N}$ and resulting $3\mathcal{N}$ random variables $(U_{i,1}, U_{i,2}, U_{i,3})$; $i = 1, \ldots, \mathcal{N}$, representing coordinates of the particle centroids in $\mathscr{D}'$; and (3) four random constituent properties E_p, E_m, ν_p, ν_m. In other words, an input random vector $\boldsymbol{R} = \{Z_{p,1}, \ldots, Z_{p,M}, \mathcal{N}, (U_{1,1}, U_{1,2}, U_{1,3}), \ldots, (U_{\mathcal{N},1}, U_{\mathcal{N},2}, U_{\mathcal{N},3}), E_p, E_m, \nu_p, \nu_m\}^T \in \mathbb{R}^N$ characterizes uncertainties from all sources in an FGM, where the dimension $N = M + 3\mathcal{N} + 5$ is an integer-valued random variable and is completely described by its joint probability density function (PDF) $f_{\boldsymbol{R}}(\boldsymbol{r})$, where $\boldsymbol{r}$ is a realization of $\boldsymbol{R}$.

2.2. Crack-driving forces and reliability

A major objective of stochastic fracture-mechanics analysis is to find probabilistic characteristics of crack-driving forces, such as SIFs $K_I(\boldsymbol{R})$, $K_{II}(\boldsymbol{R})$, and $K_{III}(\boldsymbol{R})$ for modes I–III, respectively, due to random input $\boldsymbol{R}$. For a given input sample, a standard FEA solves the discretized weak form (Eq. (2)), leading to the calculation of SIFs by standard interaction integrals [14].

Let $y(\boldsymbol{R})$ describe a generic crack-driving force or a relevant performance function involving SIFs for a given FGM fracture problem of interest. Suppose that a failure is defined when the crack propagation is initiated at a crack tip on the crack front, *i.e.*, when the effective SIF $K_{\text{eff}}(\boldsymbol{R}) = \bar{h}(K_I(\boldsymbol{R}), K_{II}(\boldsymbol{R}), K_{III}(\boldsymbol{R})) > K_{Ic}$, where $\bar{h}$ depends on the selected mixed-mode fracture criterion [15] and K_{Ic} is a relevant mode-I fracture toughness of the material measured in terms of SIF. This requirement cannot be satisfied with certainty, since K_I, K_{II}, and K_{III} are all dependent on $\boldsymbol{R}$, which is random, and K_{Ic} itself may be a random variable or field. Hence, the fracture performance of an FGM should be evaluated by the conditional reliability or its complement, the conditional probability of fracture initiation $P_F(K_{Ic})$, defined as the multifold integral

$$P_F(K_{Ic}) := P[y(\boldsymbol{R}) < 0] := \int_{\mathbb{R}^N} \mathbb{I}_y(\boldsymbol{r}) f_{\boldsymbol{R}}(\boldsymbol{r})\, d\boldsymbol{r}, \tag{7}$$

where

$$y(\boldsymbol{R}) = K_{Ic} - \bar{h}(K_I(\boldsymbol{R}), K_{II}(\boldsymbol{R}), K_{III}(\boldsymbol{R})) \tag{8}$$

is a multivariate performance function that depends on the random input $\boldsymbol{R}$ and $\mathbb{I}_y(\boldsymbol{r})$ is an indicator function such that $\mathbb{I}_y(\boldsymbol{r}) = 1$ if $y(\boldsymbol{r}) < 0$ and $\mathbb{I}_y(\boldsymbol{r}) = 0$ if $y(\boldsymbol{r}) > 0$. The evaluation of the multidimensional integral in Eq. (7), either analytically or numerically, is not possible because the total number of random variables N is large, $f_{\boldsymbol{R}}(\boldsymbol{r})$ is generally non-Gaussian, and $y(\boldsymbol{r})$ is a highly nonlinear function of $\boldsymbol{r}$. Crude Monte Carlo simulation to estimate the fracture-initiation probability is computationally burdensome, if not prohibitive; therefore, alternative stochastic methods are essential for providing both accurate and efficient solutions.

The effort in conducting probabilistic fracture analysis of FGM is influenced by two primary sources: (1) deterministic computing of SIFs, which requires expensive FEA for a given input sample and (2) stochastic computing of SIFs, which involves uncertainty propagation in a high-dimensional stochastic system. A new moment-modified PDD method in conjunction with a concurrent multiscale fracture model developed in this work reduces computational demand from both sources.

3. Concurrent multiscale analysis

The FGM microstructure schematically illustrated in Fig. 1a contains discontinuities in material properties at the interfaces between the matrix and particles. At the crack-front region, discrete material property information derived from the microstructure is required for calculating the crack-tip fields accurately. However, far away from the crack-front, where the effect of the crack-tip singularity vanishes rapidly, individual constituent material properties may not be needed, and an appropriately derived continuous, effective material property should suffice. Therefore, a concurrent multiscale analysis, where the material representation is discrete at the crack-front region and continuous elsewhere, leading to a combined micromechanical and macromechanical stress analysis should provide a more efficient solution of crack-tip fields than a microscale analysis that is solely based on discrete material representation everywhere.

As depicted in Fig. 1b, consider an arbitrary, three-dimensional, bounded subdomain $\overline{\mathscr{D}} \subseteq \mathscr{D}$ surrounding the crack front. The number of particles falling in $\overline{\mathscr{D}}$ is $\overline{\mathscr{N}} := \overline{\mathscr{N}}(\overline{\mathscr{D}})$, where $\overline{\mathscr{D}} \subset \mathbb{R}^3$ is a bounded subset such that points of $\overline{\mathscr{N}}$ falling in $\mathbb{R}^3 \setminus \overline{\mathscr{D}}$ do not contribute to particles in $\overline{\mathscr{D}}$. The integer-valued random variable $\overline{\mathscr{N}}$ also follows a Poisson distribution with the same intensity function $\lambda(\boldsymbol{x})$ derived from Eq. (6). The subdomain $\overline{\mathscr{D}}$, once defined, is statistically filled with particles, whereas the remaining subdomain $\mathscr{D} \setminus \overline{\mathscr{D}}$ is assigned a continuously varying effective elasticity tensor $\overline{\boldsymbol{C}}(\boldsymbol{x})$, obtained from a suitable micromechanical homogenization [16]. According to the concurrent multiscale model, Eq. (2) is discretized and solved using

$$\boldsymbol{C}(\boldsymbol{x}) \cong \begin{cases} \boldsymbol{C}^{(p)}, & \text{if } (\boldsymbol{x} \in \overline{\mathscr{D}} \text{ and } \boldsymbol{x} \in \mathscr{D}_p), \\ \boldsymbol{C}^{(m)}, & \text{if } (\boldsymbol{x} \in \overline{\mathscr{D}} \text{ and } \boldsymbol{x} \in \mathscr{D}_m), \\ \overline{\boldsymbol{C}}(\boldsymbol{x}), & \text{if } \boldsymbol{x} \in \mathscr{D} \setminus \overline{\mathscr{D}}, \end{cases} \tag{9}$$

where discontinuity in material properties at the interfaces between $\overline{\mathscr{D}}$ and $\mathscr{D} \setminus \overline{\mathscr{D}}$ and between $\mathscr{D}_p$ and $\mathscr{D}_m$ exist, rendering calculation of SIF difficult. To overcome this problem, consider a small, bounded subdomain $\mathscr{D}_\epsilon \subset \overline{\mathscr{D}}$ surrounding a crack tip of interest with coordinate $\boldsymbol{x}_{\text{tip}}$, depicted in Fig. 1c, such that material properties of either the particle or the matrix phase are assigned in $\mathscr{D}_\epsilon$. The result is a slight modification of the elasticity tensor, for instance,

$$\boldsymbol{C}(\boldsymbol{x}) \cong \begin{cases} \boldsymbol{C}^{(p)}, & \text{if } (\boldsymbol{x} \in \mathscr{D}_\epsilon \text{ and } \boldsymbol{x}_{\text{tip}} \in \mathscr{D}_p) \text{ or if } (\boldsymbol{x} \in \overline{\mathscr{D}} \setminus \mathscr{D}_\epsilon \text{ and } \boldsymbol{x} \in \mathscr{D}_p), \\ \boldsymbol{C}^{(m)}, & \text{if } (\boldsymbol{x} \in \mathscr{D}_\epsilon \text{ and } \boldsymbol{x}_{\text{tip}} \in \mathscr{D}_m) \text{ or if } (\boldsymbol{x} \in \overline{\mathscr{D}} \setminus \mathscr{D}_\epsilon \text{ and } \boldsymbol{x} \in \mathscr{D}_m), \\ \overline{\boldsymbol{C}}(\boldsymbol{x}), & \text{if } \boldsymbol{x} \in \mathscr{D} \setminus \overline{\mathscr{D}}, \end{cases} \tag{10}$$

yielding a locally homogeneous material representation, *i.e.*, $\boldsymbol{C}(\boldsymbol{x})$ is either $\boldsymbol{C}^{(p)}$ or $\boldsymbol{C}^{(m)}$, but constant for $\boldsymbol{x} \in \mathscr{D}_\epsilon$. Consequently, the mixed-mode SIFs at that crack tip ($\boldsymbol{x}_{\text{tip}} \in \mathscr{D}_\epsilon$) are readily calculated from [14,17]

$$K_i \cong \begin{cases} \frac{1}{2} M_p^{(1,i)} E_p^*, & \text{if } \boldsymbol{x}_{\text{tip}} \in \mathscr{D}_p, \\ \frac{1}{2} M_m^{(1,i)} E_m^*, & \text{if } \boldsymbol{x}_{\text{tip}} \in \mathscr{D}_m, \end{cases}; \; i = I, II, \tag{11}$$

and

$$K_{III} \cong \begin{cases} M_p^{(1,III)} \mu_p, & \text{if } \boldsymbol{x}_{\text{tip}} \in \mathscr{D}_p, \\ M_m^{(1,III)} \mu_m, & \text{if } \boldsymbol{x}_{\text{tip}} \in \mathscr{D}_m, \end{cases} \tag{12}$$

where $M_p^{(1,i)}$ and $M_m^{(1,i)}$ are the associated interaction integrals for mode i ($i = I, II, III$), when $\boldsymbol{C}(\boldsymbol{x}) = \boldsymbol{C}^{(p)}, \boldsymbol{x} \in \mathscr{D}_\epsilon$ and $\boldsymbol{C}(\boldsymbol{x}) = \boldsymbol{C}^{(m)}, \boldsymbol{x} \in \mathscr{D}_\epsilon$, respectively, provided that their domains of integration lie within $\mathscr{D}_\epsilon$. For plane stress conditions, $E_j^* = E_j$, and for plane strain conditions or three-dimensional problems, $E_j^* = E_j/(1 - \nu_j^2)$, where E_j denotes the elastic modulus, ν_j denotes the Poisson's ratio, and $\mu_j = E_j/2(1 + \nu_j)$ is the shear modulus. The subscripts $j = p$ and $j = m$ refer to particle and matrix, respectively. Since the interaction integrals vary along the crack front, the SIFs also depend on the crack-tip location. In Eq. (10), the size of $\mathscr{D}_\epsilon$ should be comparable to the microstructural length scale but large enough for the interaction integrals and SIFs to be calculated accurately. Further details of the concurrent multiscale model, including verification with a full microscale model, are available in the authors' prior work on two-dimensional FGMs [9].

The stochastic analysis employing the concurrent multiscale model has the random input vector $\boldsymbol{R} = \{Z_{p,1}, \ldots, Z_{p,M}, \overline{\mathscr{N}}, (U_{1,1}, U_{1,2}, U_{1,3}), \ldots, (U_{\overline{\mathscr{N}},1}, U_{\overline{\mathscr{N}},2}, U_{\overline{\mathscr{N}},3}), E_p, E_m, \nu_p, \nu_m\}^T \in \mathbb{R}^N$, where $N = M + 3\overline{\mathscr{N}} + 5$. If $\overline{\mathscr{D}} \subset \mathscr{D}$, then $\overline{\mathscr{N}} < \mathscr{N}$, resulting in a dimension reduction in stochastic multiscale analysis.

4. Moment-modified polynomial dimensional decomposition method

Let $(\Omega, \mathscr{F}, P)$ be a complete probability space, where Ω is a sample space, $\mathscr{F}$ is a σ-field on Ω, and $P : \mathscr{F} \to [0, 1]$ is a probability measure. With $\mathscr{B}^N$ representing the Borel σ-field on $\mathbb{R}^N$, consider an $\mathbb{R}^N$-valued independent random vector $\{\boldsymbol{R} = \{R_1, \ldots, R_N\}^T : (\Omega, \mathscr{F}) \to (\mathbb{R}^N, \mathscr{B}^N)\}$, which describes uncertain input from the FGM microstructure and constituent elastic properties described in the preceding section. The probability law of $\boldsymbol{R}$ is completely defined by the joint PDF $f_{\boldsymbol{R}}(\boldsymbol{r}) = \Pi_{i=1}^{i=N} f_i(r_i)$, where $f_i(r_i)$ is the PDF of R_i defined on the corresponding probability triple $(\Omega_i, \mathscr{F}_i, P_i)$. Let $\mathscr{L}_2(\Omega_i, \mathscr{F}_i, P_i)$ be a Hilbert space that is equipped with a set of complete orthonormal bases $\{\psi_{ij}(r_i);\ j = 0, 1, \ldots\}$, which is consistent with the probability measure of R_i. For example, classical orthonormal polynomials, including Hermite, Legendre, and Jacobi polynomials, can be used when R_i follows Gaussian, uniform, and Beta probability distributions, respectively [18].

Let $y(\boldsymbol{R})$, a real-valued, measurable transformation on $(\Omega, \mathscr{F})$, define a SIF or relevant performance function that depends on the SIFs of a given FGM fracture problem. Using orthonormal polynomial bases and Fourier-polynomial expansions of component functions, an S-variate ($1 \leqslant S \leqslant N$) approximation from the PDD of $y(\boldsymbol{R})$ is [18]

$$\tilde{y}_S(\boldsymbol{R}) \cong y_0 + \sum_{i=1}^{N} \sum_{j=1}^{m} \alpha_{ij} \psi_{ij}(R_i) + \sum_{i_1, i_2 = 1; i_1 < i_2}^{N} \sum_{j_2=1}^{m} \sum_{j_1=1}^{m} \beta_{i_1 i_2 j_1 j_2} \psi_{i_1 j_1}(R_{i_1}) \psi_{i_2 j_2}(R_{i_2}) + \cdots + \sum_{i_1, \ldots, i_S = 1; i_1 < \cdots < i_S}^{N} \sum_{j_S=1}^{m} \cdots \sum_{j_1=1}^{m} C_{i_1 \cdots i_S j_1 \cdots j_S} \times \prod_{s=1}^{S} \psi_{i_s j_s}(R_{i_s}), \tag{13}$$

where

$$y_0 := \int_{\mathbb{R}^N} y(\boldsymbol{r}) f_{\boldsymbol{R}}(\boldsymbol{r})\, d\boldsymbol{r} = \mathbb{E}[y(\boldsymbol{R})], \tag{14}$$

$$\alpha_{ij} := \int_{\mathbb{R}^N} y(\boldsymbol{r}) \psi_{ij}(r_i) f_{\boldsymbol{R}}(\boldsymbol{r})\, d\boldsymbol{r} = \mathbb{E}[y(\boldsymbol{R}) \psi_{ij}(R_i)], \tag{15}$$

$$\beta_{i_1 i_2 j_1 j_2} := \int_{\mathbb{R}^N} y(\boldsymbol{r}) \psi_{i_1 j_1}(r_{i_1}) \psi_{i_2 j_2}(r_{i_2}) f_{\boldsymbol{R}}(\boldsymbol{r})\, d\boldsymbol{r} = \mathbb{E}[y(\boldsymbol{R}) \psi_{i_1 j_1}(R_{i_1}) \psi_{i_2 j_2}(R_{i_2})], \tag{16}$$

$$\vdots$$

$$C_{i_1 \cdots i_S j_1 \cdots j_S} = \int_{\mathbb{R}^N} y(\boldsymbol{r}) \prod_{s=1}^{S} \psi_{i_s j_s}(r_{i_s}) f_{\boldsymbol{R}}(\boldsymbol{r})\, d\boldsymbol{r} = \mathbb{E}\left[y(\boldsymbol{R}) \prod_{s=1}^{S} \psi_{i_s j_s}(R_{i_s}) \right] \tag{17}$$

are the expansion coefficients and $1 \leqslant m \leqslant \infty$ is the largest order of orthogonal polynomials. The right side of Eq. (13), for $S = N$, converges to $y(\boldsymbol{R})$ in the mean square sense as $m \to \infty$. Once the embedded coefficients $y_0,\ \alpha_{ij},\ \beta_{i_1 i_2 j_1 j_2},\ \ldots,\ C_{i_1 \cdots i_S j_1 \cdots j_S}$

are calculated, as described in a forthcoming section, Eq. (13) furnishes an approximate but explicit map $\tilde{y}_S : \mathbb{R}^N \to \mathbb{R}$ that can be viewed as a surrogate of the exact map $y : \mathbb{R}^N \to \mathbb{R}$, which describes the input-output relationship from the FGM fracture-mechanics simulation. Therefore, any probabilistic characteristic of $y(\boldsymbol{R})$, including its statistical moments and fracture-initiation probabilities, can be easily estimated by performing Monte Carlo simulation of $\tilde{y}_S(\boldsymbol{R})$ rather than that of $y(\boldsymbol{R})$.

4.1. Calculation of coefficients

4.1.1. Monte carlo simulation

Consider L independent samples $\boldsymbol{r}^{(l)} = \left\{r_1^{(l)}, \ldots, r_N^{(l)}\right\}^T \in \mathbb{R}^N;\ l = 1, \ldots, L$ of the input vector $\boldsymbol{R}$ that can be generated to estimate the coefficients

$$y_0 \cong \frac{1}{L}\sum_{l=1}^{L} y\left(\boldsymbol{r}^{(l)}\right), \tag{18}$$

$$\alpha_{ij} \cong \frac{1}{L}\sum_{l=1}^{L} y\left(\boldsymbol{r}^{(l)}\right)\psi_{ij}\left(r_i^{(l)}\right), \tag{19}$$

$$\beta_{i_1 i_2 j_1 j_2} \cong \frac{1}{L}\sum_{l=1}^{L} y\left(\boldsymbol{r}^{(l)}\right)\psi_{i_1 j_1}\left(r_{i_1}^{(l)}\right)\psi_{i_2 j_2}\left(r_{i_2}^{(l)}\right), \tag{20}$$

$$\vdots$$

$$C_{i_1 \cdots i_S j_1 \cdots j_S} \cong \frac{1}{L}\sum_{l=1}^{L} y\left(\boldsymbol{r}^{(l)}\right)\prod_{s=1}^{S}\psi_{i_s j_s}\left(r_{i_s}^{(l)}\right). \tag{21}$$

Therefore, Eq. (13) becomes

$$\begin{aligned}\tilde{y}_S(\boldsymbol{R}) \cong{}& \frac{1}{L}\sum_{l=1}^{L} y\left(\boldsymbol{r}^{(l)}\right) + \sum_{i=1}^{N}\sum_{j=1}^{m}\left(\frac{1}{L}\sum_{l=1}^{L} y\left(\boldsymbol{r}^{(l)}\right)\psi_{ij}\left(r_i^{(l)}\right)\right)\psi_{ij}(R_i) + \sum_{i_1,i_2=1;i_1<i_2}^{N}\sum_{j_2=1}^{m}\\ &\times\sum_{j_1=1}^{m}\left(\frac{1}{L}\sum_{l=1}^{L} y\left(\boldsymbol{r}^{(l)}\right)\psi_{i_1 j_1}\left(r_{i_1}^{(l)}\right)\psi_{i_2 j_2}\left(r_{i_2}^{(l)}\right)\right)\psi_{i_1 j_1}(R_{i_1})\psi_{i_2 j_2}(R_{i_2}) + \cdots\\ &+ \sum_{i_1,\ldots,i_S=1;i_1<\cdots<i_S}^{N}\sum_{j_S=1}^{m}\cdots\sum_{j_1=1}^{m}\left(\frac{1}{L}\sum_{l=1}^{L} y\left(\boldsymbol{r}^{(l)}\right)\prod_{s=1}^{S}\psi_{i_s j_s}\left(r_{i_s}^{(l)}\right)\right)\prod_{s=1}^{S}\psi_{i_s j_s}(R_{i_s}),\end{aligned} \tag{22}$$

generating the univariate or bivariate approximation of $y(\boldsymbol{R})$ by selecting $S = 1$ or $S = 2$, respectively.

The Monte Carlo integration to calculate the coefficients is approximate when $L < \infty$ and the standard errors in calculating the coefficients are proportional to the standard deviations of the integrands given in Eqs. (14)–(17) divided by $\sqrt{L}$ [19]. Therefore, the error by Monte Carlo integration can be reduced by either increasing the sample size L or decreasing the variance of the integrand. If random sampling of the integrand produces a large variance (*e.g.*, when y has rapid changes in the domain of interest, especially in sign), the error becomes unacceptably large. Therefore, depending on the nature of the function y, additional samples are required to achieve reduced error. Since an FGM fracture analysis requires expensive finite-element calculations to obtain samples of $y(\boldsymbol{R})$ for given samples of random input, increasing the sample size may render the calculation of coefficients prohibitively expensive. Another way to improve the accuracy of Monte Carlo integration with a relatively small number of samples is to reduce the variance of the integrand. In this work, an additive control variate method [19,20] was utilized toward this end.

4.1.2. Control variate

Consider a multivariate integral for the determination of the coefficients in Eqs. (15)–(17). For example, using the additive control variate technique, α_{ij} in Eq. (15) can be rewritten as

$$\alpha_{ij} = \int_{\mathbb{R}^N}[y(\boldsymbol{r}) - h(\boldsymbol{r})]\psi_{ij}(r_i)f_{\boldsymbol{R}}(\boldsymbol{r})\,d\boldsymbol{r} + \int_{\mathbb{R}^N} h(\boldsymbol{r})\psi_{ij}(r_i)f_{\boldsymbol{R}}(\boldsymbol{r})\,d\boldsymbol{r}, \tag{23}$$

where $h(\boldsymbol{r})$ is a control variate such that (1) $y(\boldsymbol{r})$ and $h(\boldsymbol{r})$ are similar over the entire domain of integration and (2) the integral $\int_{\mathbb{R}^N} h(\boldsymbol{r})\psi_{ij}(r_i)f_{\boldsymbol{R}}(\boldsymbol{r})\,d\boldsymbol{r}$ can be obtained analytically. The first term in Eq. (23) has a small variance when $y(\boldsymbol{r})$ and $h(\boldsymbol{r})$ are linearly related through

$$h(\boldsymbol{r}) = y(\boldsymbol{r}) + b, \tag{24}$$

where b is a constant. Assuming that the second term in Eq. (23) is known analytically, the variance in Eq. (23) comes only from the first term. Since $y(\boldsymbol{r})$ and $h(\boldsymbol{r})$ are similar, *i.e.*, $b \approx 0$, one can expect the variance of $[y(\boldsymbol{R}) - h(\boldsymbol{R})]\psi_{ij}(R_i)$ to be less than the variance of $y(\boldsymbol{R})\psi_{ij}(R_i)$. Using Monte Carlo integration to evaluate the first integration in Eq. (23) yields

$$\alpha_{ij} \cong \frac{1}{L}\sum_{l=1}^{L}\left[y\left(\boldsymbol{r}^{(l)}\right) - h\left(\boldsymbol{r}^{(l)}\right)\right]\psi_{ij}\left(r_i^{(l)}\right) + \int_{\mathbb{R}^N} h(\boldsymbol{r})\psi_{ij}(r_i)f_{\boldsymbol{R}}(\boldsymbol{r})\,d\boldsymbol{r}, \tag{25}$$

which is expected to give better accuracy than that given by Eq. (19). However, for any arbitrary function $y(\boldsymbol{r})$, there is no general way to find an analytical expression for $h(\boldsymbol{r})$, and it may even be impossible. Therefore, the use of Eq. (25) employing an analytical expression for $h(\boldsymbol{r})$ is often not practical, especially when $y(\boldsymbol{r})$ is obtained implicitly from FEA.

An alternative approach is to exploit the PDD of $y(\boldsymbol{r})$ to approximate $h(\boldsymbol{r})$. In this regard, consider an S-variate approximation of $y(\boldsymbol{r})$ to generate the qth approximation

$$h^{(q)}(\boldsymbol{r};N) = y_0 + \sum_{i=1}^{N}\sum_{j=1}^{m}\alpha_{ij}^{(q)}\psi_{ij}(r_i) + \sum_{i_1,i_2=1;i_1<i_2}^{N}\sum_{j_2=1}^{m}\sum_{j_1=1}^{m}\beta_{i_1i_2j_1j_2}^{(q)}\psi_{i_1j_1}(r_{i_1})\psi_{i_2j_2}(r_{i_2}) + \cdots + \sum_{i_1,\ldots,i_S=1;i_1<\cdots<i_S}^{N}\sum_{j_S=1}^{m}\cdots\sum_{j_1=1}^{m}C_{i_1\cdots i_Sj_1\cdots j_S}^{(q)}\prod_{s=1}^{S}\psi_{i_sj_s}(r_{i_s}) \tag{26}$$

of $h(\boldsymbol{r})$, where the argument N of $h^{(q)}$ denotes the total number of random variables involved (upper limit of the outer sums) and $q = 0,1,2,\ldots$. Then, the estimated coefficients are

$$\alpha_{ij}^{(q)} = \begin{cases} \frac{1}{L}\sum_{l=1}^{L} y(\boldsymbol{r}^{(l)})\psi_{ij}\left(r_i^{(l)}\right), \text{ if } q=0, \\ \frac{1}{L}\sum_{l=1}^{L}\left[y(\boldsymbol{r}^{(l)}) - h^{(q-1)}(\boldsymbol{r}^{(l)};N)\right]\psi_{ij}\left(r_i^{(l)}\right) + \alpha_{ij}^{(q-1)}, \text{ if } q=1,2,\ldots, \end{cases} \tag{27}$$

$$\beta_{i_1i_2j_1j_2}^{(q)} = \begin{cases} \frac{1}{L}\sum_{l=1}^{L} y(\boldsymbol{r}^{(l)})\psi_{i_1j_1}\left(r_{i_1}^{(l)}\right)\psi_{i_2j_2}\left(r_{i_2}^{(l)}\right), \text{ if } q=0, \\ \frac{1}{L}\sum_{l=1}^{L}\left[y(\boldsymbol{r}^{(l)}) - h^{(q-1)}(\boldsymbol{r}^{(l)};N)\right]\psi_{i_1j_1}\left(r_{i_1}^{(l)}\right)\psi_{i_2j_2}\left(r_{i_2}^{(l)}\right) + \beta_{i_1i_2j_1j_2}^{(q-1)}, \text{ if } q=1,2,\ldots, \end{cases} \tag{28}$$

$$\vdots$$

$$C_{i_1\cdots i_Sj_1\cdots j_S}^{(q)} = \begin{cases} \frac{1}{L}\sum_{l=1}^{L} y(\boldsymbol{r}^{(l)})\prod_{s=1}^{S}\psi_{i_sj_s}\left(r_{i_s}^{(l)}\right), \text{ if } q=0, \\ \frac{1}{L}\sum_{l=1}^{L}\left[y(\boldsymbol{r}^{(l)}) - h^{(q-1)}(\boldsymbol{r}^{(l)};N)\right]\prod_{s=1}^{S}\psi_{i_sj_s}\left(r_{i_s}^{(l)}\right) + C_{i_1\cdots i_Sj_1\cdots j_S}^{(q-1)}, \text{ if } q=1,2,\ldots. \end{cases} \tag{29}$$

With each new iteration in Eq. (26), $|y(\boldsymbol{r}) - h(\boldsymbol{r})|$ decreases as the coefficients are corrected based on the difference between $y(\boldsymbol{r})$ and $h(\boldsymbol{r})$. When $y(\boldsymbol{r}) = h(\boldsymbol{r})$, the first terms in Eqs. (27)–(29) become zero for $q > 0$ and no further iteration is necessary. Therefore, the iteration can be terminated by the conditions $\left|\alpha_{ij}^{(q)} - \alpha_{ij}^{(q-1)}\right| < \epsilon$, $\left|\beta_{ij}^{(q)} - \beta_{ij}^{(q-1)}\right| < \epsilon, \ldots, \left|C_{i_1\cdots i_Sj_1\cdots j_S}^{(q)} - C_{i_1\cdots i_Sj_1\cdots j_S}^{(q-1)}\right| < \epsilon$, where ϵ is a user-defined tolerance. Note that the same samples of $y(\boldsymbol{R})$ are used in all iterations, requiring no additional response calculations. Therefore, converged values of the expansion coefficients from Eqs. (27)–(29) are obtained with little additional effort.

4.2. Moment modification

The stochastic fracture analysis employing the concurrent multiscale model involves the random input vector $\boldsymbol{R} = \{Z_{p,1},\ldots,Z_{p,M},\overline{\mathscr{N}},(U_{1,1},U_{1,2},U_{1,3}),\ldots,(U_{\overline{\mathscr{N}},1},U_{\overline{\mathscr{N}},2},U_{\overline{\mathscr{N}},3}),E_p,E_m,\nu_p,\nu_m\}^T \in \mathbb{R}^N$, where finding the PDF for the particle location coordinates $\{(U_{i,1},U_{i,2},U_{1,3})\}$; $i = 1,\ldots,\overline{\mathscr{N}}$ is not trivial. Therefore, a straightforward application of the PDD method is very difficult, if not impossible, as the method requires orthonormal bases corresponding to the PDF of all input random variables involved. An alternative but approximate approach, referred to as the *moment-modified polynomial dimensional decomposition method*, was developed to circumvent this problem, and is described as follows.

Recall that $y(\boldsymbol{r}) = y(r_1,\ldots,r_N)$ represents either a SIF or a performance function that depends on SIFs. In general, the objective is to evaluate the probabilistic characteristics of a generic output response $y(\boldsymbol{R}) \in \mathbb{R}$, when the probability distribution of the random input $\boldsymbol{R} \in \mathbb{R}^N$ is prescribed. The newly developed moment-modified PDD method for stochastic fracture analysis of FGMs involves the following three-step algorithm:

- Step 1: Generate L samples $y(\boldsymbol{r}^{(l)})$, $l = 1,\ldots,L$, of the random output $y(\boldsymbol{R})$ by employing the concurrent multiscale fracture model described in Section 3. The output samples $y(\boldsymbol{r}^{(l)})$, $l = 1,\ldots,L$, contain effects of all random variables, including particle locations considered in the multiscale model.
- Step 2: Define $\overline{\boldsymbol{R}} = \{Z_{p,1},\ldots,Z_{p,M},E_p,E_m,\nu_p,\nu_m\}^T \in \mathbb{R}^{\overline{N}}$; $\overline{N} = M + 4$ as the truncated input random vector, which excludes variables describing particle locations. Using L samples of $y(\boldsymbol{R})$ from Step 1 and a truncated control variate $h^{(q)}(\overline{\boldsymbol{r}};\overline{N})$ in Eq. (26), calculate the PDD coefficients from Eqs. (27)–(29) for $i,\ i_1,\ i_2,\ i_3,\ \ldots = 1,\ \ldots,\ \overline{N}$ and $j, j_1, j_2, j_3, \ldots = 1, \ldots, m$. Therefore, the $\overline{N}$-truncation of the S-variate polynomial decomposition becomes

$$\bar{y}_S(\overline{\boldsymbol{R}}) = \frac{1}{L}\sum_{l=1}^{L} y(\boldsymbol{r}^{(l)}) + \sum_{i=1}^{\overline{N}}\sum_{j=1}^{m}\left(\frac{1}{L}\sum_{l=1}^{L} y(\boldsymbol{r}^{(l)})\psi_{ij}\left(\bar{r}_i^{(l)}\right)\right)\psi_{ij}(\overline{R}_i) + \sum_{i_1,i_2=1;i_1<i_2}^{\overline{N}}\sum_{j_2=1}^{m} \times \sum_{j_1=1}^{m}\left(\frac{1}{L}\sum_{l=1}^{L} y(\boldsymbol{r}^{(l)})\psi_{i_1j_1}\left(\bar{r}_{i_1}^{(l)}\right)\psi_{i_2j_2}\left(\bar{r}_{i_2}^{(l)}\right)\right)\psi_{i_1j_1}(\overline{R}_{i_1})\psi_{i_2j_2}(\overline{R}_{i_2}) + \cdots + \sum_{i_1,\ldots,i_S=1;i_1<\cdots<i_S}^{\overline{N}}\sum_{j_S=1}^{m}\cdots\sum_{j_1=1}^{m}\left(\frac{1}{L}\sum_{l=1}^{L} y(\boldsymbol{r}^{(l)})\prod_{s=1}^{S}\psi_{i_sj_s}\left(\bar{r}_{i_s}^{(l)}\right)\right)\prod_{s=1}^{S}\psi_{i_sj_s}(\overline{R}_{i_s}). \tag{30}$$

Since $\overline{\boldsymbol{R}}$ is a subvector of $\boldsymbol{R}$, $\bar{y}_S(\overline{\boldsymbol{R}})$ cannot fully capture the effect of the variability from particle locations.

- Step 3: Estimate the mean-variance pairs

$$\mu := \mathbb{E}[y(\boldsymbol{R})] \cong \frac{1}{L}\sum_{l=1}^{L}\left[y(\boldsymbol{r}^{(l)})\right]; \quad \sigma^2 := \mathbb{E}[y(\boldsymbol{R})-\mu]^2 \cong \frac{1}{L}\sum_{l=1}^{L}\left[y(\boldsymbol{r}^{(l)})-\mu\right]^2 \tag{31}$$

and

$$\bar{\mu} := \mathbb{E}[\bar{y}_S(\overline{\boldsymbol{R}})] \cong \frac{1}{L}\sum_{l=1}^{L}\left[\bar{y}_S(\overline{\boldsymbol{r}}^{(l)})\right]; \quad \bar{\sigma}^2 := \mathbb{E}[\bar{y}_S(\overline{\boldsymbol{R}})-\bar{\mu}]^2 \cong \frac{1}{L}\sum_{l=1}^{L}\left[\bar{y}_S(\overline{\boldsymbol{r}}^{(l)})-\bar{\mu}\right]^2 \tag{32}$$

of $y(\boldsymbol{R})$ and $\bar{y}_S(\overline{\boldsymbol{R}})$, respectively, both calculated from the existing samples of $y(\boldsymbol{R})$. Postulate that the sample properties of $(\bar{y}_S-\mu)/\sigma$ and $(\bar{y}_S-\bar{\mu})/\bar{\sigma}$ are the same, yielding yet another approximation,

$$\tilde{y}_S(\boldsymbol{R}) \cong \mu + \frac{\sigma}{\bar{\sigma}}\left[\bar{y}_S(\overline{\boldsymbol{R}})-\tilde{\mu}\right], \tag{33}$$

without requiring additional FEA.

Eq. (33) provides a heuristic, but convenient, approximation of $\tilde{y}_S(\boldsymbol{R})$ in Eq. (22) without having to include orthonormal polynomial bases associated with random particle locations.

Since the material at a crack tip ($\boldsymbol{x}_{\text{tip}}$) on the crack front can either be that of the particle or the matrix with a possibly significant mismatch between constituent properties, jumps (discontinuities) may occur in a relevant fracture response. Therefore, two separate stochastic analyses, one with the crack tip in the particle phase and the other with the crack tip in the matrix phase, are required for the moment-modified PDD method. Consider two variants of $\tilde{y}_S(\boldsymbol{R})$, $\tilde{y}_{S,p}(\boldsymbol{R})$ and $\tilde{y}_{S,m}(\boldsymbol{R})$, and their $\overline{N}$-truncated S-variate approximations, $\bar{y}_{S,p}(\overline{\boldsymbol{R}})$ and $\bar{y}_{S,m}(\overline{\boldsymbol{R}})$, that can be generated depending on whether the crack tip is in the particle or in the matrix, respectively. Correspondingly, let $\mu_p, \sigma_p^2; \mu_m, \sigma_m^2;\ \bar{\mu}_p, \bar{\sigma}_p^2$; and $\bar{\mu}_m; \bar{\sigma}_m^2$ be the pairs of second-moment statistics of $\tilde{y}_{S,p}(\boldsymbol{R})$, $\tilde{y}_{S,m}(\boldsymbol{R})$, $\bar{y}_{S,p}(\overline{\boldsymbol{R}})$, and $\bar{y}_{S,m}(\overline{\boldsymbol{R}})$, respectively. Then, an S-variate approximation of a discontinuous stochastic response from FGM fracture analysis becomes

$$\tilde{y}_S(\boldsymbol{R}) \cong \begin{cases} \mu_p + \frac{\sigma_p}{\bar{\sigma}_p}\left[\bar{y}_{S,p}(\overline{\boldsymbol{R}})-\tilde{\mu}_p\right], & \text{if } \boldsymbol{x}_{\text{tip}} \in \mathscr{D}_p, \\ \mu_m + \frac{\sigma_m}{\bar{\sigma}_m}\left[\bar{y}_{S,m}(\overline{\boldsymbol{R}})-\tilde{\mu}_m\right], & \text{if } \boldsymbol{x}_{\text{tip}} \in \mathscr{D}_m. \end{cases} \tag{34}$$

By Monte Carlo sampling of $\tilde{y}_S(\boldsymbol{R})$ in Eq. (34), the probabilistic characteristics of SIFs, including the conditional probability of fracture initiation, can be easily estimated. This sampling should not be confused with crude Monte Carlo simulation, which requires finite-element calculation of $y(\boldsymbol{r}^{(l)})$ for any input sample $\boldsymbol{r}^{(l)}$ and can, therefore, be expensive or even prohibitive, particularly when the sample size needs to be very large for estimating small probabilities. In contrast, the Monte Carlo simulation embedded in the PDD method requires evaluations of simple analytical functions that stem from an S-variate approximation $\tilde{y}_S(\boldsymbol{R})$. Therefore, an arbitrarily large sample size can be accommodated in the PDD method.

4.3. Computational effort

The moment-modified PDD method using the additive control variate requires finite-element evaluations of L samples $y(\boldsymbol{r}^{(l)})$; $l = 1, \ldots, L$, of $y(\boldsymbol{R})$ to determine the coefficients $y_0,\ \alpha_{ij},\ \beta_{i_1i_2j_1j_2}, \ldots$, for $i,\ i_1,\ i_2, \ \ldots = 1, \ \ldots, \ \overline{N}$ and $j, j_1, j_2, \ldots = 1, \ldots, m$. The iterative scheme involving the additive control variate for estimating the expansion coefficients does not require additional samples of $y(\boldsymbol{R})$. Therefore, the computational effort required by the proposed method comes primarily from conducting L FEA. However, due to the discrete nature of material property at a crack tip on the crack front, L samples or FEA are required for each of two stochastic fracture analyses – one for the matrix material at the crack tip and other for the particle material at the crack tip. Therefore, a total of $2L$ output samples or FEA are required by the proposed method.

For a generic stochastic problem, pre-selecting the sample size L is not easy. Therefore, progressively larger values of L should be tried in order to determine the minimum value of L. Furthermore, L depends on S in the S-variate approximation. From the authors' experiences, L increases with S. Therefore, a larger sample size should be expected for the bivariate ($S = 2$) approximation than for the univariate ($S = 1$) approximation.

4.4. Verification

The moment-modified PDD method provides approximate solutions; therefore, an evaluation of its accuracy with respect to a reference solution – for instance, the results from crude Monte Carlo simulation – is necessary. Since crude Monte Carlo simulation is not practical for analyzing three-dimensional media, a two-dimensional FGM specimen, previously examined by the authors [9], was selected to conduct the verification.

Consider a 16 cm × 16 cm, two-phase, FGM specimen that contains randomly dispersed, fully penetrable, circular, silicon carbide (SiC) particles with a common radius of 0.48 cm in an aluminum (Al) matrix, as shown in Fig. 2. The specimen contains a horizontally placed, 8 cm long edge-crack with the crack tip location $\boldsymbol{x}_{\text{tip}} = \{8,8\}^T$ cm and is subjected to a far-field tensile stress $\sigma^{\infty} = 1$ kN/cm^2 and a far-field shear stress $\tau^{\infty} = 1$ kN/cm^2. A plane strain condition is assumed. The random input vector $\boldsymbol{R}$ describing random microstructure and constituent elastic properties and their statistical characteristics are the same as those defined in the previous study [9]. The objective here is to calculate the conditional probability of fracture initiation, $P_F(K_{Ic}) := P[\bar{h}(K_I(\boldsymbol{R}), K_{II}(\boldsymbol{R})) > K_{Ic}]$, where the effective SIF $\bar{h}(K_I(\boldsymbol{R}), K_{II}(\boldsymbol{R}))$ is derived from the maximum circumferential stress criterion [15]. The probability of fracture initiation was calculated by two stochastic methods: (1) the proposed moment-modified PDD method, including the univariate ($S = 1$) and bivariate ($S = 2$) versions, and (2) crude Monte Carlo simulation. For the moment-modified PDD method, the fracture analysis was performed using the concurrent multiscale model, where the subdomain $\overline{\mathscr{D}}$ is a 16κ cm × 16κ cm square with the center coinciding with the crack tip and two cases of $\kappa = 0.25$ and 0.5, corresponding to small and large subdomain sizes, respectively. The truncated input random vector $\overline{\boldsymbol{R}}$, which contains eight standard Gaussian variables, $Z_{p,1}, \ldots, Z_{p,8}$, and four lognormal variables, E_p, E_m, ν_p, ν_m, was mapped into uniform random variables $U(0,1)$, and shifted third-order ($m = 3$) Legendre polynomials were used for the associated polynomial basis functions. The sample sizes for estimating the expansion coefficients for each crack-tip condition are $L = 1000$ for the univariate method and $L = 5000$ for the bivariate method. Therefore, the total number of FEA is 2000 for the univariate method and 10,000 for the bivariate method. The sample size for stochastic analyses by the moment-modified PDD method and crude Monte Carlo simulation is 10,000. For crude Monte Carlo simulation, the fracture analysis was conducted using both the concurrent multiscale and microscale models. The microscale model constitutes a brute-force approach that employs a discrete particle-matrix system in the entire domain $\mathscr{D}$. Further details are available elsewhere [9].

Fig. 3a shows how the conditional probability of fracture initiation $P_F(K_{Ic})$ of the FGM specimen varies as a function of the fracture toughness K_{Ic} for the small subdomain ($\kappa = 0.25$). The three plots (dashed line, dash-dot-dotted line, dash-dotted line) in Fig. 3a were obtained from three different probabilistic methods – univariate PDD, bivariate PDD, and crude Monte Carlo methods – each employing the concurrent multiscale model for fracture analysis. The results from the proposed univariate and bivariate methods closely match the crude Monte Carlo results, even for small probabilities in the tail region. These three plots are also reasonably close to the reference solution (solid line) obtained by crude Monte Carlo simulation using the microscale model for fracture analysis. Fig. 3b, which depicts similar plots for the large subdomain ($\kappa = 0.5$), reveals excellent agreement between the PDD methods (univariate or bivariate) and the reference solution. The accuracy of the PDD methods with respect to the reference solution improves when κ increases from 0.25 to 0.5, as expected.

Comparing the computational efforts required by the probabilistic methods or fracture models involved in producing the plots in Fig. 3a and b suggests that the univariate method, which requires 2000 FEA, is five time more efficient than crude Monte Carlo simulation involving 10,000 FEA, both employing the concurrent multiscale model for fracture analysis. In contrast, the bivariate method requires 10,000 FEA, the same number of analyses involved in crude Monte Carlo simulation, and

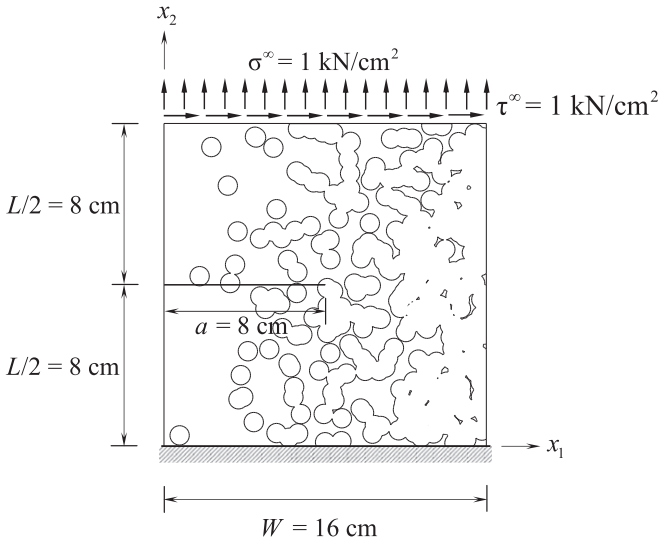

Fig. 2. A two-dimensional, edge-cracked FGM specimen under a mixed-mode deformation.

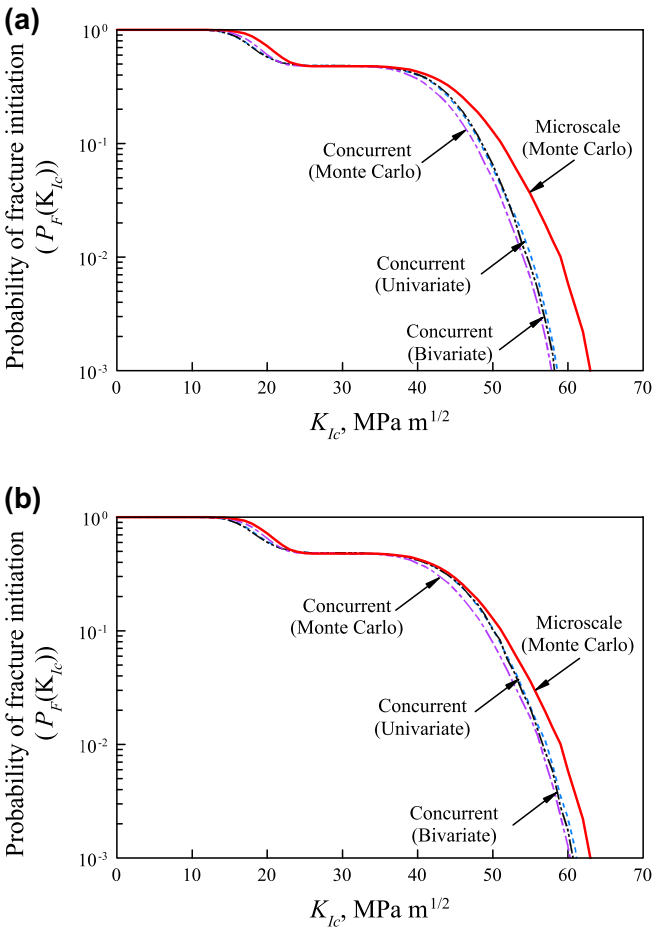

Fig. 3. Conditional probability of fracture initiation of a two-dimensional FGM specimen by the PDD and crude Monte Carlo methods: (a) $\kappa = 0.25$ and (b) $\kappa = 0.5$.

therefore results in no computational savings. If the required sample size for crude Monte Carlo simulation is larger than 10,000 – for instance, when calculating probabilities lower than 10^{-3} – only then will a reduction in computational cost be achieved, even with the bivariate approximation. Nonetheless, the univariate method, which is almost as accurate as the bivariate method or crude Monte Carlo simulation, is significantly more economical than the two latter methods.

5. A numerical example

Consider a three-dimensional FGM specimen with domain $\mathscr{D} = (16\text{ m} \times 16\text{ cm} \times 4\text{ cm})$, which contains randomly dispersed, fully penetrable, spherical, SiC particles in an Al matrix, as shown in Fig. 4a. All particles have the same volume with a common radius of 0.48 cm. The specimen contains a horizontally placed, 8 cm – long, 4 cm – deep, planar edge-crack and is subjected to a far-field tensile stress $\sigma^{\infty} = 1\text{ kN/cm}^2$, an in-plane shear stress $\tau_i^{\infty} = 1\text{ kN/cm}^2$, and an out-of-plane shear stress $\tau_o^{\infty} = 0.6\text{ kN/cm}^2$. A fixed boundary condition comprising zero displacements in all three directions is applied at the bottom surface. The cuboid subdomains $\mathscr{D}' = (16.96\text{ cm} \times 16.96\text{ cm} \times 4.96\text{ cm})$, $\overline{\mathscr{D}} = (16\kappa\text{ cm} \times 16\kappa\text{ cm} \times 4\text{ cm})$, and $\overline{\mathscr{D}'} = (16\kappa + 0.96\text{ cm} \times 16\kappa + 0.96\text{ cm} \times 4.96\text{ cm})$, where $\kappa = 0.2$ or 0.4, all have centers coinciding with the center of the specimen domain. The selected values of κ are guided by the conditional failure probability curves in Fig. 3, which barely change when increasing κ from 0.25 to 0.5.

The particle volume fraction $\phi_p(x_1)$, which varies only along the horizontal coordinate x_1, is a one-dimensional, inhomogeneous, Beta random field with marginal PDF $[1/B(q,t)]\phi_p^{q-1}(1-\phi_p)^{t-1}$, where q and t are distribution parameters, $\Gamma(\tau) := \int_0^{\infty} \exp(-\eta)\eta^{\tau-1}\,d\eta$ is the Gamma function, and $B(q,t) := \Gamma(q)\Gamma(t)/\Gamma(q+t)$ is the Beta function. It has mean $\mu_p(x_1) = \bar{x}_1^2$ and standard deviation $\sigma_p(x_1) = 0.1\bar{x}_1(1-\bar{x}_1)$, where $\bar{x}_1 = x_1/L$, with L denoting the length of the specimen in the x_1 direction. The standardized volume fraction $\tilde{\phi}_p(x_1)$, a Beta random field with *zero* mean and *unit* variance, has covariance function $\Gamma_{\tilde{\phi}_p}(s) = \exp(-5|s|)$. The Karhunen–Loéve approximation was employed to parameterize the Gaussian image field $\alpha_p(x_1)$ of $\tilde{\phi}_p(x_1)$ into eight ($M = 8$) standard Gaussian random variables $Z_{p,1}, \ldots, Z_{p,8}$. The Karhunen–Loéve expansion was truncated after eight terms, because the eighth eigenvalue is only 4.5% of the maximum eigenvalue. For a given sample

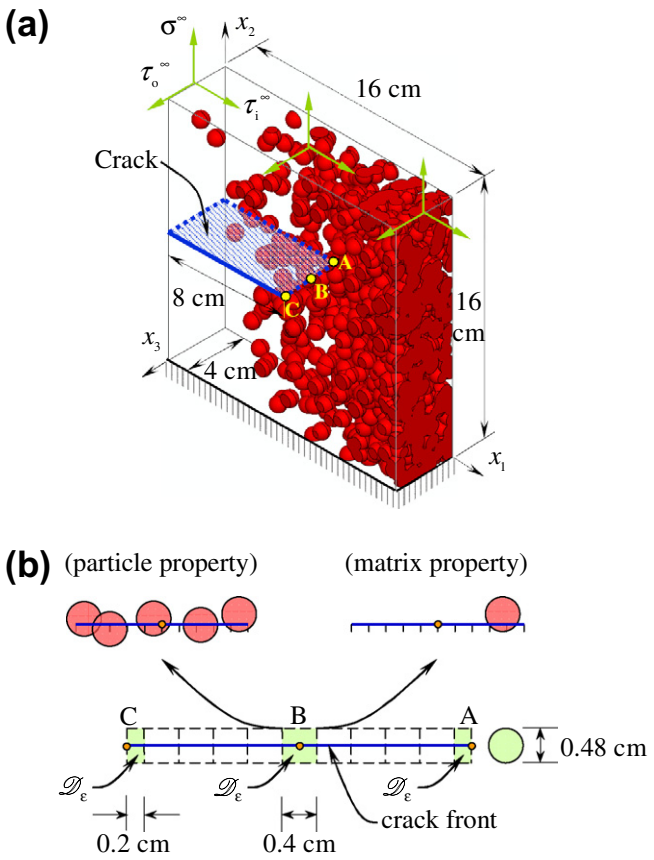

Fig. 4. A three-dimensional, edge-cracked, SiC-Al FGM specimen: (a) specimen with a sample of microstructure under a mixed-mode deformation and (b) assigning material property of $\mathscr{D}_\epsilon$.

$\varphi_p(x_1)$ of the random volume fraction $\phi_p(x_1)$, the corresponding number of particles $\overline{\mathscr{N}}$ in $\overline{\mathscr{D}}'$ is a Poisson variable and has the intensity function $\lambda(\boldsymbol{x})$ that was obtained from Eq. (6). The sample values of $\overline{\mathscr{N}}$ associated with the microstructural sample in Fig. 4a are 133 for $\kappa = 0.2$ and 223 for $\kappa = 0.4$. Correspondingly, the total numbers of random variables are 411 and 681, respectively, both representing high-dimensional stochastic systems. The material phases SiC and Al are both linear-elastic and isotropic. However, the elastic moduli E_{SiC} and E_{Al} and the Poisson's ratios ν_{SiC} and ν_{Al}, of SiC and Al, respectively, are random variables; their means, standard deviations, and probability distributions are listed in Table 1. Each component of the truncated input random vector $\overline{\boldsymbol{R}} = \{Z_{p,1}, \ldots, Z_{p,8}, E_p, E_m, \nu_p, \nu_m\}^T \in \mathbb{R}^{12}$ was mapped into a uniform random variable $U(0,1)$, and third-order ($m = 3$) shifted Legendre polynomials were employed for the associated polynomial basis functions. For the univariate PDD, $L = 1000$ random samples were used to calculate the corresponding coefficients with the control variate truncated at the univariate approximation (Eq. (26)) and a tolerance (ϵ) of 0.001 for the iterative scheme (Eqs. (26)–(29)). Due to two distinct cases of crack-tip material properties, two sets of coefficients were estimated, requiring a total of 2000 FEA by the univariate PDD method. The sample size for stochastic analysis using the univariate PDD method is 10,000. Therefore, the smallest value of the fracture-initiation probability calculated is limited to $10/10{,}000 = 10^{-3}$.

5.1. Finite element modeling

All finite-element analyses including mesh generation were conducted using the commercial code ABAQUS [17]. Figs. 5a and b present two finite-element discretizations of a sample of the three-dimensional FGM specimen employed in

Table 1
Statistical properties of constituents in SiC-Al FGM.

Elastic property[a]	Mean	Coefficient of variation, %	Probability distribution
E_{SiC}, GPa	419.2	15	Lognormal
E_{Al}, GPa	69.7	10	Lognormal
ν_{SiC}	0.19	15	Lognormal
ν_{Al}	0.34	10	Lognormal

[a] $E_p = E_{\text{SiC}}$; $E_m = E_{\text{Al}}$; $\nu_p = \nu_{\text{SiC}}$; $\nu_m = \nu_{\text{Al}}$.

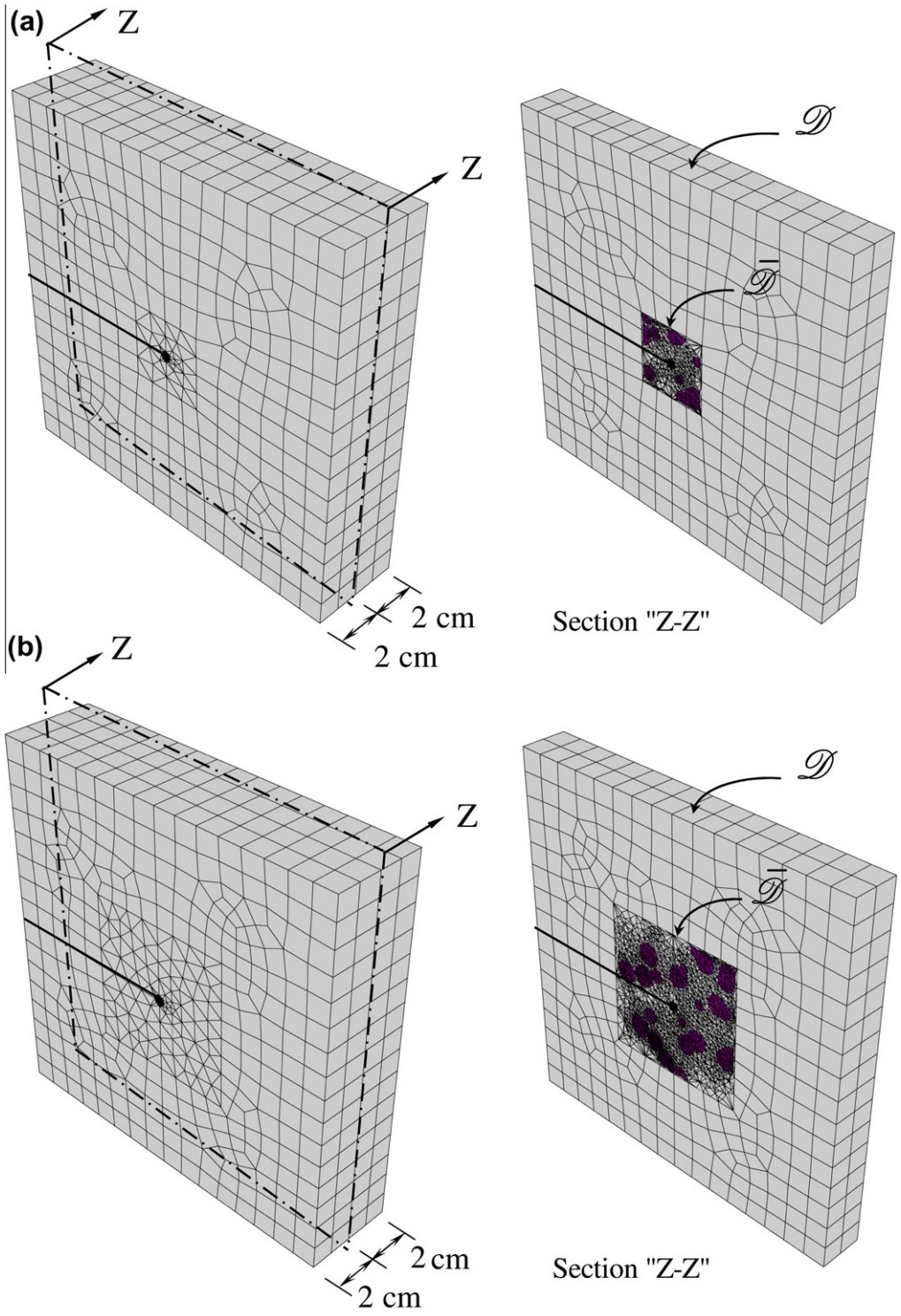

Fig. 5. Finite element discretizations of a SiC-Al FGM sample specimen employing the concurrent multiscale model: (a) $\kappa = 0.2$ (degrees of freedom = 219,540) and (b) $\kappa = 0.4$ (degrees of freedom = 864,573).

conjunction with the concurrent multiscale model with $\kappa = 0.2$ and $\kappa = 0.4$, respectively. The figures displaying finite elements in $\overline{\mathscr{D}}$ are produced by making a cut "*Z*–*Z*" from the meshed specimen along the x_1–x_2 plane at $x_3 = 2$ cm. The mesh

for the concurrent model with $\kappa = 0.2$ has 1064 20-noded, non-singular, quadratic brick (hexahedral) elements in $\mathscr{D} \setminus \overline{\mathscr{D}}$; 25,622 10-noded, non-singular, quadratic tetrahedral elements in $\overline{\mathscr{D}} \setminus \mathscr{D}_\epsilon$; and 1280 20-noded, non-singular, quadratic brick elements and 160 20-noded, quarter-point (singular), collapsed quadratic brick elements in $\mathscr{D}_\epsilon$ along the crack front. The numbers of such elements are 1076, 117,412, 1280, and 160, respectively, for $\kappa = 0.4$. The total degrees of freedom correspondingly rise from 219,540 for $\kappa = 0.2$ to 864,573 for $\kappa = 0.4$. The rapid increase in the number of degrees of freedom and, hence, the problem size with respect to κ indicates a need for efficient stochastic multiscale analysis with a subdomain that is as small as possible. Full $3 \times 3 \times 3$ and four-point Gauss quadrature rules were employed for the hexahedral and tetrahedral elements, respectively, for numerical integration. The crack faces were defined as contact surfaces due to the presence of far-field out-of-plane shear stress. However, the effects of friction due to contact on modes-II and -III fracture behaviors, if they exist, were not considered in this study.

5.2. Calculations of stress-intensity factors and reliability

The moment-modified univariate PDD method employing the concurrent multiscale fracture model was applied to calculate the probabilistic characteristics of SIFs and the probability of fracture initiation at three distinct crack tips, which are marked in Fig. 4a: crack-tip A, $\boldsymbol{x}_{\text{tip}} = \{8,8,0\}^T$ cm; crack tip B, $\boldsymbol{x}_{\text{tip}} = \{8,8,2\}^T$ cm; and crack tip C, $\boldsymbol{x}_{\text{tip}} = \{8,8,4\}^T$ cm. The crack-tip subdomains ($\mathscr{D}_\epsilon$) are 0.48 cm diameter cylinders with lengths of 0.4 cm for crack tip B and 0.2 cm for crack tip A or C, and their axes are coincident with the crack front. During Monte Carlo simulation of PDD-generated random output $\tilde{y}_S(\boldsymbol{R})$ from Eq. (34), the material property of $\mathscr{D}_\epsilon$ for a crack tip was selected by the following process (Fig. 4b): (1) define a point set comprising 11 equidistant points on the portion of the crack front inside $\mathscr{D}_\epsilon$; (2) count the numbers of points from the point set falling in $\mathscr{D}_p$ and $\mathscr{D}_m$; and (3) assign a homogeneous material property of particle (matrix) if the number of points falling in $\mathscr{D}_p$ ($\mathscr{D}_m$) is larger than the number of points falling in $\mathscr{D}_m$ ($\mathscr{D}_p$). However, when calculating the expansion coefficients of $\bar{y}_{S,p}(\overline{\boldsymbol{R}})$ or $\bar{y}_{S,m}(\overline{\boldsymbol{R}})$, the subdomains for crack tips A, B, and C were all assigned the same material property of either particle or matrix, and the remaining subdomains were assigned sample material properties, depending on the microstructural sample. This is justified because the particle volume fraction chosen varies only in the x_1 direction.

Initiation of crack growth in a three-dimensional media is a complex phenomenon because of crack-front twisting resulting from the out-of-plane tearing mode (mode-III). There is no consensus yet on when and how a crack propagates under a general mixed-mode deformation because the relation between the mode-III SIF and the tendency of the crack front to twist is unknown [21]. Therefore, due to a present lack of understanding, initiation of crack propagation in a three-dimensional configuration is generally evaluated at distinct crack tips on the crack front using two-dimensional mixed-mode (modes-I and -II) criteria, where mode-III SIF and deformation are neglected [22]. In this study, the probability of fracture initiation, defined in Eq. (7), was calculated at each crack tip using $y(\boldsymbol{R}) = K_{Ic} - \bar{h}(K_I(\boldsymbol{R}), K_{II}(\boldsymbol{R}))$, where the effective SIF $\bar{h}(K_I(\boldsymbol{R}), K_{II}(\boldsymbol{R}))$ is derived from the maximum circumferential stress criterion [15].

5.3. Results and discussions

Fig. 6a and b plot von Mises stress contours for two randomly selected FGM samples, generated using the concurrent multiscale fracture model with $\kappa = 0.2$ and $\kappa = 0.4$, respectively. The effective properties required by the multiscale model were calculated using the Mori–Tanaka approximation [16]. The overall stress responses from both samples, indicated by the contour patterns, are similar. However, there also exist differences in the local stress fields that may have profound implications in determining SIFs and eventually in reliability predictions. The results pertaining to fracture response and reliability are presented next.

5.3.1. Moments of crack-driving forces

Table 2 lists the means and coefficients of variation of K_I, K_{II}, and K_{III} by the univariate PDD method employing the concurrent multiscale fracture model with two different subdomain sizes ($\kappa = 0.2$ and 0.4). The statistics are tabulated for three crack tips A, B, and C. From Table 2, the univariate PDD method yields almost the same mean values of all three SIFs at a given crack tip when $\kappa = 0.2$ and 0.4. A slight uptick in the coefficients of variation of SIFs at a given crack tip, observed when κ is doubled, is due to a larger volume of the subdomain $\overline{\mathscr{D}}$, which captures explicit particle location information from a larger region around the crack front, thereby incorporating more variability into SIFs. Nonetheless, the second-moment statistics of SIFs obtained for $\kappa = 0.2$ and 0.4 are reasonably close to each other, indicating the usefulness of the concurrent multiscale model with the smaller subdomain for generating efficient stochastic solutions. It would be interesting to discover if the same trend holds when comparing the sample properties or probability distributions of SIFs.

While the coefficients of variation of K_I at all three crack tips are relatively uniform, K_{II} and K_{III} exhibit larger coefficients of variation at crack tip B than at crack tips A and C. This is because the modes-II and -III SIFs at crack tip B, which is surrounded by more particles than crack tip A or C, are more sensitive to the variability of particle locations than the mode-I SIF.

5.3.2. Probability densities of crack-driving forces

While the second-moment statistics are important, a more meaningful stochastic response is the PDF of a SIF. Fig. 7a–c present the predicted marginal probability densities of K_I at three crack tips A–C, respectively, obtained by the univariate PDD method and the concurrent multiscale model with $\kappa = 0.2$ and 0.4. The PDFs of K_I for all three crack tips reveal a bimodal

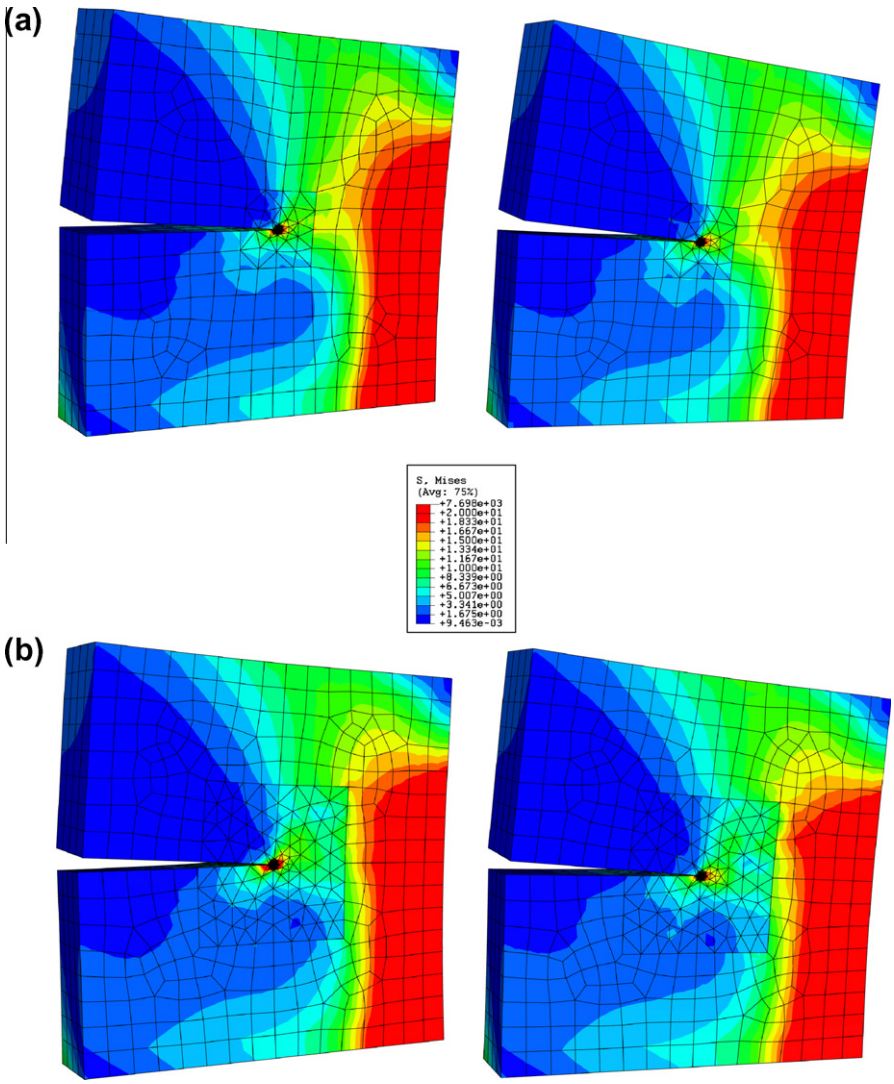

Fig. 6. von Mises stress contours for two SiC-Al FGM sample specimens employing the concurrent multiscale model: (a) $\kappa = 0.2$ and (b) $\kappa = 0.4$.

Table 2
Second-moment statistics of SIFs by the univariate PDD method.

	K_I		K_{II}		K_{III}	
Crack tip	Mean (MPa$\sqrt{\text{m}}$)	COV[a] (%)	Mean (MPa$\sqrt{\text{m}}$)	COV[a] (%)	Mean (MPa$\sqrt{\text{m}}$)	COV[a] (%)
(a) $\kappa = 0.2$						
A	36.788	23.147	−5.834	23.388	4.240	17.147
B	25.124	18.845	1.960	52.235	5.123	28.098
C	9.173	25.853	9.259	14.892	4.721	22.832
(b) $\kappa = 0.4$						
A	38.153	24.958	−5.981	25.832	4.300	17.921
B	25.936	19.982	2.009	58.648	5.371	30.086
C	9.148	28.226	9.407	15.243	4.795	22.973

[a] The coefficient of variation (COV) is standard deviation divided by mean, when mean is not zero.

shape, where the left and right parts of the density are due to major contributions from the matrix and particle phases, respectively. The sample values of K_I (horizontal co-ordinate) decrease in the positive x_3 direction along the crack front,

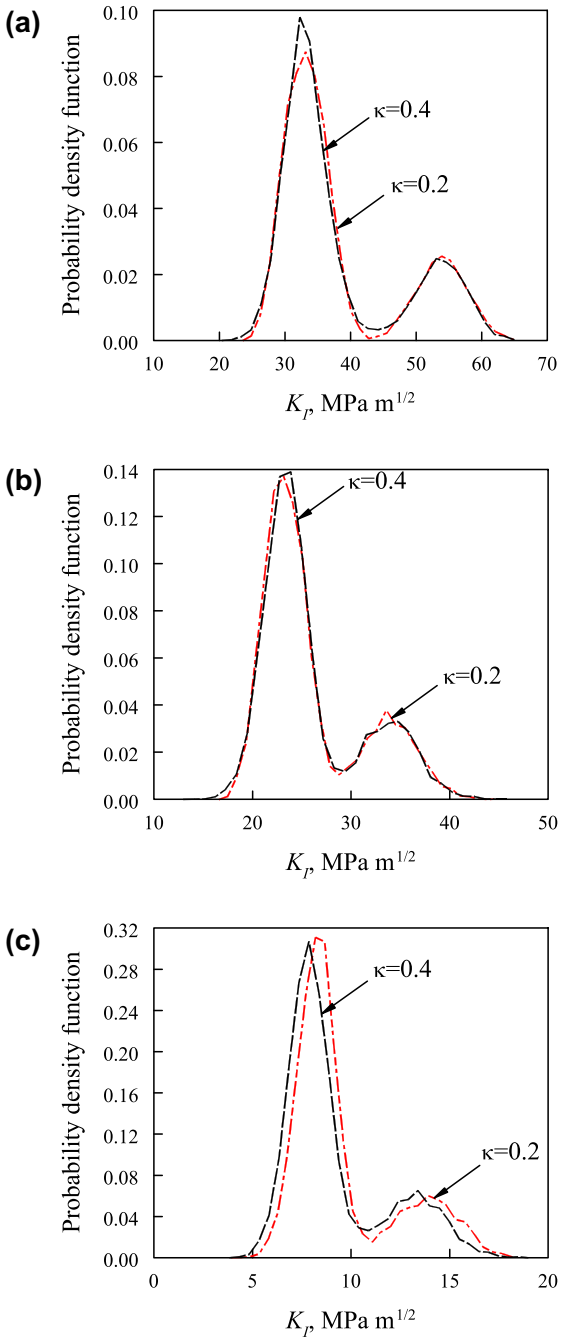

Fig. 7. Marginal probability density of K_I by the univariate PDD method at various crack tips on the crack front: (a) crack tip A; (b) crack tip B; and (c) crack tip C.

i.e., when moving from crack tip A to crack tip B to crack tip C. This is due to the far-field out-of-plane shear stress τ_o^∞ creating a bending moment about the x_1 axis, which in turn tries to close the crack faces in the x_2 direction. The tendency of closing the crack faces increases along the positive x_3 direction, lowering the SIF values at crack tip C relative to crack tip A. Correspondingly, the mean value of K_I also decreases when traversing along the crack front A–B–C, as shown in Table 2.

The marginal PDFs of K_{II} and K_{III}, obtained by the univariate PDD method and organized similarly, are displayed in Fig. 8a–c and Fig. 9a–c, respectively. Again, the probability densities are calculated at crack tips A–C and for both $\kappa = 0.2$ and 0.4. The PDFs of K_{II} at all three crack tips are unimodal, and therefore, different than those of K_I. This is because the mode-II fracture behavior is dominated more by the distribution of particles close to the crack front than by the explicit presence of material phases enclosing the crack front. Furthermore, the PDFs reveal a sign change in K_{II} when moving from

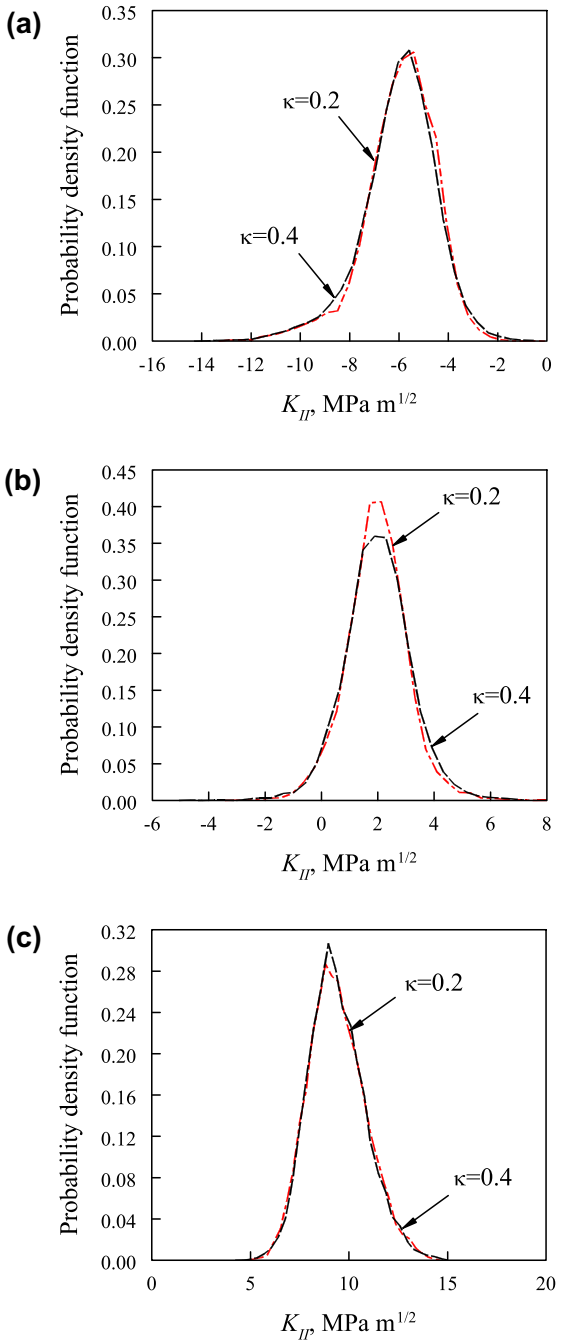

Fig. 8. Marginal probability density of K_{II} by the univariate PDD method at various crack tips on the crack front: (a) crack tip A; (b) crack tip B; and (c) crack tip C.

crack tip A (all negative samples) to crack tip C (all positive samples), while crack tip B contains both positive and negative sample values. This is due to τ_o^∞ creating a twisting moment about the x_2 axis, which in turn tries to rotate the crack faces in the $x_1 - x_3$ plane. As a result, the mean value of K_{II} also changes sign from negative to positive values at crack tips A and C, respectively, as shown in Table 2.

In contrast, the PDFs of K_{III} have either unimodal or slightly bimodal shapes. The modality of the distribution of K_{III} depends on the location of a crack tip inside the three-dimensional FGM specimen. Compared with the PDFs of K_I (Fig. 7b), the PDFs of K_{III} (Fig. 9b) at crack tip B, located at the middle of the crack front, are slightly bimodal, indicating less pronounced effect due to individual contributions from the matrix and particle phases. As a consequence, the bimodal shape

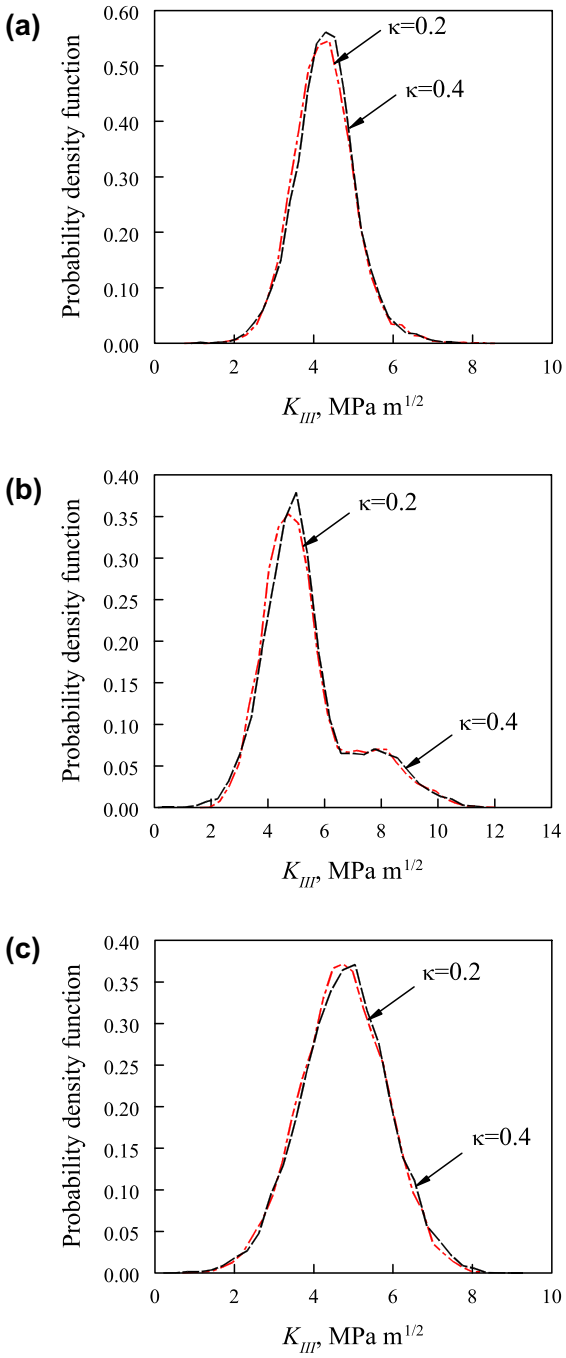

Fig. 9. Marginal probability density of K_{III} by the univariate PDD method at various crack tips on the crack front: (a) crack tip A; (b) crack tip B; and (c) crack tip C.

is lost at crack tips A and C, as they are surrounded by fewer particles than crack tip B. Therefore, the distributions of K_{III} at crack tips A and C are unimodal. However, the mean values of K_{III} remain nearly the same along the crack front, as shown in Table 2.

The insensitivity of statistical moments of SIFs with respect to κ discussed earlier also extends to the probability densities of SIFs, regardless of the fracture mode or crack tip examined. Indeed, the PDFs in Figs. 7–9 are practically identical when κ increases from 0.2 to 0.4. Therefore, stochastic multiscale analysis can be efficiently conducted using a smaller subdomain, at least in this example.

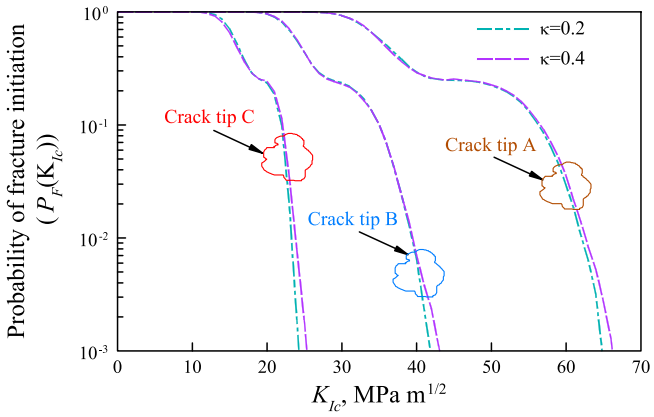

Fig. 10. Conditional probability of fracture initiation of a three-dimensional FGM specimen by the univariate PDD method.

5.3.3. Fracture reliability

Fig. 10 presents the conditional probability of fracture initiation, $P_F(K_{Ic})$: = $P[y(\boldsymbol{R}) < 0]$, of the three-dimensional FGM specimen for a given fracture toughness K_{Ic} of the crack-tip material. The results are shown for three crack tips A–C. Two cases of results were generated: $\kappa = 0.2$ and $\kappa = 0.4$, representing the small and large subdomains, respectively, of the concurrent multiscale model. In both cases, the probability of fracture initiation for a given K_{Ic} at crack tip A is significantly larger than at crack tip C, whereas the initiation probability at crack tip B assumes an intermediate value. This is caused by the out-of-plane far-field shear stress (τ_0^∞) creating a bending moment about the x_1 axis, which in turn tries to close the crack faces in the x_2 direction. The crack-opening displacement decreases along the positive x_3 direction, rendering progressively smaller initiation probabilities when moving along the crack front A–B–C. Increasing the value of κ from 0.2 to 0.4 does not alter the fracture probability curves appreciably, even at the tail regions. This observation tallies with similar findings from analyzing cracks in two-dimensional FGMs reported in a prequel [9].

Due to markedly different fracture-initiation probabilities along the crack front, crack propagation in a three-dimensional FGM, if it occurs, is a highly complex phenomenon. The crack faces following fracture initiation are not expected to remain planar; crack front splitting and/or branching are possible. It would be intriguing to study such heterogeneity-driven crack growth phenomena within a stochastic framework. A multiscale probabilistic analysis of crack growth in a three-dimensional FGM setting is beyond the scope of the current work.

5.3.4. Computational effort

For the moment-modified univariate PDD method, Monte Carlo simulation entailing 2000 samples was conducted employing the concurrent multiscale model with $\kappa = 0.2$ and 0.4. Half of these samples involved assigning particle property at the subdomains of crack tips A–C, and the other half involved assigning matrix property at the same subdomains. Therefore, 2000 deterministic FEA were required, leading to the conditional probability curves in Fig. 10. All analyses were performed using an HP XW8400 workstation, a common desktop computer. The absolute CPU time required by concurrent multiscale analysis of a typical deterministic sample, including all pre-processing efforts, was 270 s when $\kappa = 0.2$ and 925 s when $\kappa = 0.4$. This leads to a full stochastic analysis times of approximately 6.3 and 21.4 days for $\kappa = 0.2$ and 0.4, respectively. No probabilistic analysis using the proposed method entailing concurrent multiscale models with larger subdomains ($0.4 < \kappa < 1$) or a full microscale model ($\kappa = 1$) was performed. Due to high computational demand, crude Monte Carlo simulation involving multiscale or microscale analysis is not feasible or required. Therefore, the univariate PDD method in conjunction with the concurrent multiscale model developed provides an efficient alternative to crude Monte Carlo simulation for probabilistic fracture analysis of three-dimensional FGMs.

6. Conclusions

A new moment-modified PDD method was developed for stochastic multiscale fracture analysis of three-dimensional, particle-matrix FGMs subject to arbitrary boundary conditions. The method is based on Fourier-polynomial expansions of component functions by orthonormal polynomial bases, an additive control variate in conjunction with Monte Carlo simulation for calculating the expansion coefficients, and a moment-modified random output to account for the effects of particle locations and geometry. The analysis involves a statistically inhomogeneous random microstructure of FGMs, describing particle volume fractions, number, and locations, and random constituent properties, and a two-scale concurrent multiscale algorithm including microscale and macroscale analyses for determining crack-driving forces. A verification study conducted on a two-dimensional functionally graded specimen reveals that the univariate PDD method produces the same crude Monte Carlo results with a five-fold reduction in the computational effort. In contrast, the bivariate PDD method requires the same

computational effort as crude Monte Carlo simulation, yielding no such computational savings when calculating tail probabilities equal to or larger than 10^{-3}. Therefore, stochastic multiscale analysis can be efficiently conducted using the univariate method.

To illustrate the usefulness of the proposed stochastic method, a two-phase, three-dimensional, edge-cracked, functionally graded specimen subject to mixed-mode deformation was analyzed to calculate the probabilistic characteristics of crack-driving forces and the probability of failure. The results demonstrate that (1) the statistical moments or probability distributions of crack-driving forces and the conditional probability of fracture initiation can be efficiently generated by the univariate method; (2) the probability distributions of mode-I and mode-II SIFs are respectively bimodal and unimodal at any crack tip but the distributions of mode-III SIFs change from unimodal to bimodal shapes, depending on the crack-tip location along the crack front; and (3) there exist significant variations in the probabilistic characteristics of the SIFs and the fracture-initiation probability along the crack front. Furthermore, the results are insensitive to the subdomain size from concurrent multiscale analysis, which, if selected judiciously, leads to computationally efficient estimates of the probabilistic solutions.

A stochastic analysis employing the moment-modified PDD method requires fewer deterministic FEA than crude Monte Carlo simulation. Since a single deterministic analysis of a three-dimensional configuration may come with a heavy computational price tag, the newly developed decomposition method should provide an efficient alternative to crude Monte Carlo simulation for probabilistic multiscale analysis of FGMs.

Acknowledgments

The authors would like to acknowledge financial support from the US National Science Foundation under Grant No. CMS-0409463.

References

[1] Suresh S, Mortensen A. Fundamentals of functionally graded materials. London: Institute of Materials; 1998.
[2] Rao BN, Rahman S. Mesh-free analysis of cracks in isotropic functionally graded materials. Eng Fract Mech 2003;70:1–27.
[3] Dolbow JE, Gosz M. On the computation of mixed-mode stress intensity factors in functionally graded materials. Int J Solids Struct 2002;39(9):2557–74.
[4] Kim JH, Paulino GH. Finite element evaluation of mixed-mode stress intensity factors in functionally graded materials. Int J Numer Methods Eng 2002;53(8):1903–35.
[5] Walters MC, Paulino GH, Dodds Jr RH. Interaction integral procedures for 3D curved cracks including surface tractions. Eng Fract Mech 2005;72:1635–63.
[6] Yildirim B, Dag S, Erdogan F. Three dimensional fracture analysis of FGM coatings under thermomechanical loading. Int J Fract 2005;132:369–95.
[7] Yong H, Zhou YH. Analysis of a mode III crack problem in a functionally graded coating-substrate system with finite thickness. Int J Fract 2006;141:459–67.
[8] Ferrante FJ, Graham-Brady LL. Stochastic simulation of non-gaussian/non-stationary properties in a functionally graded plate. Comput Methods Appl Mech Eng 2005;194:1675–92.
[9] Chakraborty A, Rahman S. Stochastic multiscale models for fracture analysis of functionally graded materials. Eng Fract Mech 2008;75:2062–86.
[10] Rahman S, Chakraborty A. A stochastic micromechanical model for elastic properties of functionally graded materials. Mech Mater 2007;39:548–63.
[11] Quintanilla J, Torquato S. Microstructure functions for a model of statistically inhomogeneous random media. Phys Rev E 1997;55(2):1558–65.
[12] Chakraborty A, Rahman S. A parametric study on probabilistic fracture of functionally graded composites by a concurrent multiscale method. Probabilist Eng Mech 2009;24:438–51.
[13] Stoyan D, Stoyan H. Fractals, random shapes and point fields: methods of geometrical statistics. New York: John Wiley & Sons, Inc.; 1994.
[14] Yau JF, Wang SS, Corten HT. A mixed-mode crack analysis of isotropic solids using conservation laws of elasticity. J Appl Mech 1980;47:335–41.
[15] Anderson TL. Fracture mechanics-fundamentals and applications. 3rd ed. Florida: CRC Press; 2005.
[16] Mura T. Micromechanics of defects in Solids. 2nd revised ed. Dordrecht, The Netherlands: Kluwer Academic Publishers.; 1991.
[17] ABAQUS, 2007. User's guide and theoretical manual, Version 6.7, ABAQUS Inc., Providence, RI.
[18] Rahman S. A polynomial dimensional decomposition for stochastic computing. Int J Numer Methods Eng 2008;76:972–93.
[19] Genyuan L, Rabitz H. Ratio control variate method for efficiently determining high-dimensional model representations. J Comput Chem 2006;27:1112–8.
[20] Evans M, Swartz T. Approximating integrals via Monte Carlo and deterministic methods. Oxford, New York, NY: Oxford University Press; 2000.
[21] Krysl P, Belytschko T. The element-free Galerkin method for dynamic propagation of arbitrary 3D cracks. Int. J Numer Methods Eng 1999;44:767800.
[22] FRANC3D, 2004. Concepts and users guide. Version 2.6, Cornell Fracture Group, Department of Civil and Environmental Engineering, Ithaca, NY.